Depletion of *ALMS1* affects TGF-β signalling pathway and downstream processes such as cell migration and adhesion capacity.

Brais Bea-Mascato[1,2], Elena Neira-Goyanes[1,2], Antía Iglesias-Rodríguez[1,2], Diana Valverde[1,2*]

1 CINBIO, Universidad de Vigo, 36310, Spain.

2 Grupo de Investigación en Enfermedades Raras y Medicina Pediátrica, Instituto de Investigación Sanitaria Galicia Sur (IIS Galicia Sur), SERGAS-UVIGO, Vigo, Spain

*Correspondence: Diana Valverde

CINBIO Facultad de Biología, Universidad de Vigo, Campus As Lagoas-Marcosende s/n, 36310 Vigo, Spain

Tel +34 986 811 953

Email dianaval@uvigo.es

ABSTRACT:

Background:

ALMS1 is a ubiquitous gene associated with Alström syndrome (ALMS). The main symptoms of ALMS affect multiple organs and tissues, generating at last, multi-organic fibrosis in the lungs, kidneys and liver. TGF-β is one of the main pathways implicated in fibrosis, controlling the cell cycle, apoptosis, cell migration, cell adhesion and epithelial-mesenchymal transition (EMT). Nevertheless, the role of *ALMS1* gene in fibrosis generation and other implicated processes such as cell migration or cell adhesion via the TGF- β pathway has not been elucidated yet.

Methods:

Initially, we evaluated how depletion of *ALMS1* affects different processes like apoptosis, cell cycle and mitochondrial activity in HeLa cells. Then, we performed proteomic profiling with TGF-β stimuli in HeLa ALMS1 -/- cells and validated the results by examining different EMT biomarkers using qPCR. The expression of these EMT biomarkers were also studied in hTERT-BJ-5ta ALMS1 -/-. Finally, we also evaluated the SMAD3 and SMAD2 phosphorylation and cell migration capacity in both models.

Results:

Depletion of *ALMS1* generated apoptosis resistance to thapsigargin (THAP) and C2-Ceramide (C2-C), and G2/M cell cycle arrest in HeLa cells. For mitochondrial activity, results did not show significant differences between *ALMS1 +/+* and *ALMS1 -/-*. Proteomic results showed inhibition of downstream pathways regulated by TGF-β. The protein-coding genes (PCG) were associated with processes like focal adhesion or cell-substrate adherens junction in HeLa. *SNAI1* showed an opposite pattern to what would be expected when activating the EMT in HeLa and BJ-5ta. Finally, in BJ-5ta model a reduced activation of SMAD3 but not SMAD2 were also observed. In HeLa models no alterations in the canonical TGF-β pathway were observed but both cell lines showed a reduction in migration capacity.

Conclusion:

ALMS1 has a role in controlling the cell cycle and the apoptosis processes. Moreover, the depletion of *ALMS1* affects the signal transduction through the TGF-β and other processes like the cell migration and adhesion capacity.

Keywords: ALMS1, Alström syndrome, ciliopathies, primary cilia, TGF-β, epithelial-mesenchymal transition (EMT), fibrosis, cell cycle arrest, cell migration, apoptosis.

INTRODUCTION:

ALMS1 is a ubiquitous gene with 23 exons located on chromosome 2p13. Mutations in this gene are related to Alström syndrome (ALMS; OMIM #203800), a rare, autosomal and recessive disease with a prevalence of 1-9 cases per 1.000.000 inhabitants and approximately 950 cases reported worldwide (Orphanet). The main symptoms of ALMS affect multiple organs and tissues [1], such as cone-rod retinal dystrophy, dilated cardiomyopathy (DCM) and hypertension [2], hypertriglyceridemia, type II diabetes mellitus (T2D) [3], and hepatic, renal and pulmonary dysfunction caused by multi-organic fibrosis [1], [4], which is the main cause of death in these patients.

The protein encoded by *ALMS1* plays a structural role in the eukaryotic cell centrosomes [5], a microtubule (MT)-nucleating organelle strongly related to primary cilia. The ALMS1 basal body location [5], [6] has been related to different functions controlled by the primary cilium such as centrosome cohesion, cell cycle control and endosomal trafficking [6]–[9].

Although numerous roles of ALMS1 have been described at both ciliary and extraciliary levels, the regulation of the pathways underlying these cellular processes remain unknown. Recently, our group has established the relationship between the *ALMS1* gene and the TGF-β signaling pathway [10], which could be related to the development of fibrosis in these patients [11], [12]. TGF-β is a signalling pathway regulated by clathrin-dependent endocytosis (CDE) in the pocket region of primary cilium [13], and coordinates cell cycle, apoptosis and migration processes such as epithelium-mesenchyme transition (EMT) [14]. This pathway acts in close coordination with other signalling cascades such as Wnt, Hippo, Notch, Hedgehog (Hh), mitogen-activated protein kinase (MAPK), and phosphoinositide 3-kinase (PI3K)-Akt, resulting in many cases in complex regulatory networks dependent on the primary cilium [15].

Stimulation of the TGF-β pathway can activate two main cascades: the canonical (SMAD-dependent) pathway and the non-canonical (SMAD-independent) pathway [16]. The canonical pathway is coordinated by transcription factors called R-SMAD (SMAD2 and SMAD3) which join co-SMAD (SMAD4) to activate the expression of several genes such as *SNAI1* [17], [18], a key modulator of EMT [19], [20]. This pathway is inhibited by an I-SMAD, SMAD7, which inhibits R-SMAD signalling in a variety of ways, binding to TGF-β receptors or directly in the nucleus, avoiding the binding of the R-Smad-Smad4 complex to DNA [21]. On the other hand, the non-canonical activation pathway includes a wide group of pathways such as p38 MAPK, PI3K/AKT, or Rho GTPases [16]. Recently, studies have linked the abolition of several centrosomal proteins such as ALMS1 and CEP128 to the inhibition of the SMAD-dependent canonical pathway in

82 zebrafish and various human cell types such as hTERT-RPE1 and ciliated human foreskin
83 fibroblasts (hFF) [10], [22]. However, deciphering how centrosomal proteins coordinate and
84 regulate the TGF-β signalling pathway and their downstream processes is a challenge.

85 Understanding how the absence of *ALMS1* influence cell migration and adhesion processes such
86 as EMT through the TGF-β pathway is key to understanding how the multi-organ fibrosis occurs
87 in these patients.

88 In this article, we analysed how the lack of *ALMS1* could affect different cell processes such as
89 mitochondrial activity, cell cycle, apoptosis, and signal transduction through the TGF-β pathway.
90 Moreover, we evaluated the expression pattern for different EMT biomarkers after TGF-β
91 pathway stimulation in two independent CRISPR-KO cell models (HeLa and BJ-5TA) for *ALMS1*.
92 Finally, we measured p-SMAD3 and p-SMAD2 activation and migration capacity in in the
93 presence and absence of the TGF-β1 ligand.

94 MATERIALS AND METHODS:

95 Cell culture:

96 HeLa human cervical cancer cell line from American Type Culture Collection (ATCC), hTERT BJ-
97 5ta human dermal fibroblasts (ATCC) and 293T human embryonic kidney cell line from ATCC
98 were used in this study. HeLa and 293T cells were maintained in Dulbecco's minimum essential
99 medium (DMEM, Gibco, Invitrogen, NY, USA), supplemented with 10% fetal bovine serum (FBS)
100 (Gibco, Invitrogen, NY, USA) and 2% penicillin/streptomycin (P/S) (Gibco, Invitrogen, NY, USA).
101 In the case of BJ-5ta line, cells were maintained in DMEM:199, supplemented with 10% of FBS,
102 2% P/S and Hygromycin B (0.01mg/mL). All cell lines were grown at 37°C with 5% CO_2 for up to
103 one month. After this, the cells were discarded, and a new culture was started.

104

105 ## Crispr assay and edition validation:

106 HeLa cells were edited with a dual episomal system for homology directed repair (HDR) (Santa
107 Cruz Biotechnology, Inc., Dallas, USA). Cells were transfected with Lipofectamine 2000 (Thermo
108 Fisher, Waltham, EE. UU) with 3 gRNAs directed to *ALMS1* exons 1 and 3 (Supplementary Table
109 S1) following the manufacture´s protocol. After plasmid transfection, cells were selected with
110 puromycin (1 µg/mL) for 5 days.

111 **Supplementary Table S1.** gRNAs of the constructs used for gene editing. The forward and
112 reverse sequences are shown in the table. The red colour represents the base pairs added for
113 ligation in the plasmid.

ID	Cell line	Exon	Forward primer (gRNA sequence 5' - 3')	Reverse primer (5' - 3')	Strand	PAM	On-target Score	Off-Target Score
gRNA 1 HeLa	HeLa	1	GCCCCCGCAGCACCGCTACT	AGTAGCGGTGCTGCGGGGGC	+	CGG	51,4	89,3
gRNA 2 HeLa	HeLa	1	TCCGCTCGCCCTCCGAGTAG	CTACTCGGAGGGCGAGCGGA	-	CGG	56	91
gRNA 3 HeLa	HeLa	3	TTCTCACATTAAACCTAGTC	GACTAGGTTTAATGTGAGAA	-	TGG	29,1	76,7
gRNA 1 BJ	hTERT-BJ-5ta	3	CACCGCCTAGTCTGGGATGTATCCA	aaacTGGATACATCCCAGACTAGGCC	-	AGG	56,2	77,1
gRNA 2 BJ	hTERT-BJ-5ta	3	CACCGAACAGAAGAGATCTCTGTT	aaacAACAGAGATCTCTTCTGTTC	-	GGG	63,3	58,1

114

115 BJ-5ta cells were edited using a lentivirus system according to the protocol described by Sanjana
116 et al [23], with some modifications. Check supplemental material for more information. After
117 lentiviral transduction, cells were selected with puromycin (1µg/mL) for 5 days.

118 Surviving cells were expanded and isolated to obtain individual clones. Of the isolation was
119 performed using Fluorescence-Activated Cell Sorting (FACS) with Hoechst (BD Bioscience, San
120 José, USA) in the flow cytometer FACS ARIA III (BD Bioscience, San José, USA). Inhibition of gene
121 expression was validated by qPCR in a StepOnePlus instrument (Thermo Fisher, Waltham, USA).
122 A commercial probe TaqMan® Gene Expression Assays (Hs00367316_m1) and PrimeTime® qPCR
123 Primer Assays (Hs.PT.56a.488948) were used to detect *ALMS1* in the HeLa and BJ-5ta models,
124 respectively.

125

126 ## Mitochondrial activity assay:

127 Mitochondrial activity was evaluated using Presto Blue reagent (Thermo Fisher, Waltham, USA).
128 Wild type (*ALMS1* +/+) and Hela Knockout cells (*ALMS1* -/-) were seeded in 96-well plates by
129 triplicate in concentrations from 5 x 10^4 to 1.5 x 10^3 cells per well. The plates were incubated for
130 24 hours as previously described. After incubation, 10 µL of Presto Blue were added to each well
131 and cells were incubated for 2 hours. Next, the plate was centrifuged at 1500 rpm for 5 min and
132 the supernatant was transferred to a fluorescence plate (Corning, NY, EE. UU). Finally, the plates
133 were measured in the Envision plate reader (Perkin-Elmer, Waltham, USA). This experiment was
134 repeated 3 times on different days.

135 ## Apoptosis assay:

136 The apoptosis assay was performed in flat-bottom 96-well plates. HeLa *ALMS1* +/+ and *ALMS1* -
137 /- cells were seeded in triplicate at a concentration of 3 x 10^4 cells/per well and incubated 24
138 hours in DMEM 2%P/S and 2%FBS before treatment. Next, apoptotic stimuli were added at final
139 concentration of 100 nM for thapsigargin (THAP) and 25µM for C2-ceramide (C2-C) in plates,
140 followed by incubation at 37ºC for 24-48 hours respectively. After that, cells were washed twice
141 with 100 µL PBS. 50 µL trypsin was added per well and the plate was incubated for 5 min at 37°C.
142 After that, trypsin was inactivated with 50 µL DMEM 10% FBS 2% P/S, and cells were transferred
143 to 96-well plates with U bottom. The plate was centrifugated at 1500 rpm for 5 min, the
144 supernatant was discarded, and the cells were resuspended in 200 µL biding buffer with 2µL 7-
145 AAD and 2µL annexin V-FITC (Biolegend Inc, San Diego, CA, USA). The plate was incubated for
146 15 min in darkness and measured in the flow cytometer FC 500 (Beckman-Coulter, Brea, CA,
147 USA). This experiment was repeated 3 times on different days.

148 ## Cell cycle assay:

149 To determine cell cycle alterations, we studied sub-populations in the HeLa *ALMS1* -/- model
150 with Hoechst staining (BD Bioscience, San José, USA). *ALMS1* +/+ and *ALMS1* -/- cells were
151 seeded in a 6-well plate at a concentration of 3 X 10^5 cells/per well and incubated overnight. The
152 next day, 1µL Hoechst staining was added to the medium and the plate was incubated for 1
153 hour. Then, the medium was removed, cells were washed twice with 1 mL PBS per well, and
154 trypsinised following the protocol described above. Cells were resuspended in PBS and analysed
155 in the flow cytometer FACS ARIA III.

156

157 ## Protein extraction for proteomic profiling:

158 HeLa cells were seeded in 6-well plates by triplicate in DMEM 2% P/S, 2%FBS and incubated
159 overnight for serum starvation. One the next day, cells were stimulated with rhTGF-β1 (2ng/mL;
160 R&D Systems; 240-B) for 24 hours. After that, DMEM was removed, and wells were washed
161 twice with PBS. Cells were scrapped in PBS. Then, cells were pelleted at 11000 rpm for 5 min,
162 and 100 µL of RIPA Buffer were added to each sample. Samples were incubated on ice for 20
163 min in constant agitation. Finally, cell debris was pelleted by centrifugation for 30 min at 12000
164 rpm and 4 °C. Samples were aliquoted and stored at -80 °C until the next protocol's step. Protein
165 quantification was performed by Bradford microplate assay (Bio-Rad, Hercules, USA).

166 ## Protein concentration, reduction, and alkylation:

167 Initially, 20 µg of each sample was concentrated and stained with Coomassie in a 12% SDS-PAGE
168 gel. Bands were cut and faded. Band distinction was performed by adding 100 µL of ammonium
169 bicarbonate 25mM/50% acetonitrile and incubated 20 min. This step was repeated 4 times.
170 After distinction, the supernatant was removed and 100 µL of ammonium bicarbonate 25mM-
171 50% EtOH was added to samples, and incubated for 20 min. Then, the supernatant was removed
172 and 100 µL EtOH was added and incubated for 15 min. In the next step, 200 µL 10mM DTT in
173 ammonium bicarbonate were added and samples were incubated for 1 hour at 56°C. Then, DTT
174 solution was removed and 200 µL iodoacetamide (IAA) 55mM in 50 mM ammonium bicarbonate
175 was added. Samples were incubated again for 30 min at room temperature. Finally, the
176 supernatant was removed, 200 µL ammonium bicarbonate 50mM were added and samples
177 were incubated for 15 min.

178 ## Protein digestion:

179 After reduction and alkylation, samples were digested. 100 µL ammonium bicarbonate 25mM-
180 50% acetonitrile (ACN) was added to each sample and incubated for 30 min. The supernatant
181 was removed and 100 µL ACN 100% was added and incubated for 10 min. The supernatant was
182 removed again and 15 µL Trypsin in ammonium bicarbonate 25mM were added to each sample.
183 Samples were maintained at 4°C for 30 min. Finally, trypsin was removed, 5 µL ammonium
184 bicarbonate 25 mM were added, and samples were incubated overnight.

185 ## Peptide extraction:

186 40 µL of trifluoroacetic acid (TFA) 0.5% were added to each sample and incubated for 30 min at
187 room temperature. Then, we added 20 µL ACN 100% in each 1.5 mL tube and incubated for 15

188 min at 37°C. Finally, the samples were dried in a speed-vac at 45°C for 1 hour and stored at -
189 20°C until the analysis.

190 Mass Spectrometry and bioinformatic analysis:

191 Samples were resuspended in 24 µL formic acid 0.1%. Then, 10 µL were injected into the HPLC
192 (LC-ESI-MS/MS workflow using a C18 precolumn). Samples were analysed in a mass
193 spectrophotometry Orbitrap ELITE (Thermo-Fisher, Waltham, USA) in long chromatography
194 mode (4 hours). After that, protein identification was performed in the database
195 UniProtKB/TrEMBL for humans, using the Proteome Discoverer software. Downstream analysis
196 was performed with the R package Differential Enrichment analysis of Proteomics data (DEP
197 package) [24]. Finally, Go Terms analysis was performed with Clusterprofiler package [25], and
198 results were visualized with GOplot package [26]. All the code for the analysis was deposited in
199 the GitHub repository (https://github.com/BreisOne/CRISPR_Hela_KO_Alms1).

200 The mass spectrometry proteomics data have been deposited in the ProteomeXchange
201 Consortium via the PRIDE [27] partner repository with the dataset identifier PXD024964.

202 RNA extraction and RT-PCR:

203 HeLa cells were seeded in 6-well plates at a concentration of $2x10^5$ by triplicate in DMEM 2%P/S
204 and 2%FBS and were incubated overnight for serum starvation. The next day, cells were
205 stimulated with rhTGF-β1 (2 ng/mL) for 24, 48 and 72 hours. DMEM was removed and wells
206 were washed twice with PBS. Cells were scraped in PBS and collected in a 1.5 mL tubes. For the
207 RNA extraction, the NYZ total RNA isolation kit (NYZtech, Lisboa, Portugal) was used following
208 the manufacture´s protocol.

209 After RNA elution, the sample concentrations were measured with Nanodrop (Thermo Fisher,
210 Waltham, USA). Next, 300 ng of RNA were retrotranscribed to cDNA using the NZY First-Strand
211 cDNA Synthesis kit (NYZtech, Lisboa, Portugal) following the manufacture´s protocol.

212 For the experiment with the BJ-5ta line, the same protocol was followed but using DMEM:199
213 and stimulating for 24 and 48 hours only.

214 qPCR expression analysis:

215 Samples were prepared in 96-well plates (Thermo Fisher, Waltham, EE. UU) adding 1µL of each
216 primer, 12.5µL of PowerUp SYBR Green Master Mix (Thermo Fisher, Waltham, EE. UU), 1µL of
217 cDNA and 4.5µL of H_20_d in a final volume of 20 µL per well. qPCRs were performed in
218 StepOnePlus instrument using the following, cycling conditions: 10 min at 95°C, 40 cycles of 15

219 s at 95°C and 1 min at 60°C.Primers were synthesized on demand (IDT) (Supplementary Table
220 S2). Samples were analysed by technical triplicates for each sample and gene. Cts for technical
221 triplicates were averaged using the geometric mean and ΔΔCT method was applied for the
222 normalization, using 2 housekeeping (HK) genes (*ALAS1* and *YWHAZ*).

223 **Supplementary Table S2.** Sequences of the primers used for the evaluation of qPCR expression
224 of epithelial-mesenchymal transition markers and genotyping of the Knockout lines.

Gene symbol	Forward primer	Reverse primer
POSTN	CACTCTTTGCTCCCACCAAT	GCCACTTTGTCTCCCATGAT
CDH2	CCTCCAGAGTTTACTGCCATGAC	GTAGGATCTCCGCCACTGATTC
ACTA2	CTATGCCTCTGGACGCACAACT	CAGATCCAGACGCATGATGGCA
SNAI1	GCTGCAGGACTCTAATCCAGAGTT	GACAGAGTCCCAGATGAGCATTG
TWIST1	GCCAGGTACATCGACTTCCTCT	TCCATCCTCCAGACCGAGAAGG
EDIL3	GCGAATGGAACTTCTTGGCTGTG	GAGCGTTCTGAAGATGCTGGAG
VIM	AGGCAAAGCAGGAGTCCACTGA	ATCTGGCGTTCCAGGGACTCAT
DSP	TGACAGACCGCTGGCAAAGGAT	GGCGTTTAGCATCATAGAGCCAC
ALMS1 (Exon1)	GCACTGCGCCTAAGCTG	gttgggggtggaggctg
ALMS1 (Exon3)	cagttaatgacttagcatgttttcct	ctttccccttttgagttaagga
ALMS1 (Exon 1 -3)	GAGCGAGACACCAACATGGA	ATTGCGTCAATATGCCCTCCT

225

226 Wound healing assay:

227 BJ-5ta and HeLa (WT and KO) were seeded in a 24-well plate (6 wells per cell line and genotype)
228 at a concentration of $1x10^5$ and cultured until a 90-95% of confluence. Cells were serum-
229 starvated (2%FBS for HeLa cells) for 24 hours. After that, rh-TGF-β1 (2 ng/mL) was added to half
230 of the wells and a wound performed with a 200 µL pipette tip. Cells were incubated at 37°C 5%
231 CO_2 and images were taken at 0 and 24 hours with the microscope inverted Nikon TiU. Images
232 were analysed with the imageJ program [28] and the plugin developed by Suarez-Armendo et al
233 [29]. Finally, the percentage of closure was measured with respect to the wound area at time 0.

234 SMADs activation assays:

235 For p-SMADs/SMADs activation assays, BJ-5ta and HeLa (WT and KO) cells were plated in 100mm
236 dishes (Corning, NY, USA) and incubated in DMEM:199 2P/S% without FBS and DMEM 2% P/S,
237 2%FBS for 24 hour, respectively. Then, TGF-β pathway were stimulated adding rhTGF-β1 ligand
238 at 2 ng/mL (final concentration in dish) for 0, 10, 30, and 90 min in BJ-5ta and 0 and 30 min in
239 HeLa. After stimulation, cells were washed 3 times with PBS, harvested using a scraper, and
240 centrifuged in a Sigma® 1–14 K at 4°C, 7,400×g for 10 min. Then, pellets were lysed on ice for 10
241 min in 200 µL of RIPA lysis buffer containing 1 mM sodium orthovanadate as phosphatase

242 inhibitor (Sigma-Aldrich, Misuri, USA) and 0.1% (v/v) protease inhibitor cocktail (Merck,
243 Darmstadt, Germany). Lysates were centrifuged at 4°C, 14,500×g for 30 min, and the
244 supernatant was collected in 1.5mL low binding tubes (Thermo Fisher, Waltham, EE. UU). The
245 remaining pellet was discarded. Quantification was performed using Bradford assay in
246 microplates with Bio-Rad protein assay and samples were stored at -80°C until analysis.

247 SDS-PAGE, Western Blotting, and Quantification:

248 A total amount of 20µg from each sample were mixed with 6,25µL of Laemmli Buffer 4X (Biorad,
249 Hércules, EE.UU), 1,25µL β-mercaptoethanol (BME) and a volume of H_2O_d up to a final volume
250 of 25µL. Then, the mixes were boiled at 97ºC for 5 min and loaded in a Mini-PROTEAN® TGX™
251 Precast Gel (Biorad, Hércules, EE.UU) at 12% acrylamide/bis-acrylamide. The gel was migrated
252 for 1 hour at 150V. Then, gels were transferred to a 0.2 µm PVDF membrane using the Trans-
253 Blot Turbo transfer system (Biorad, Hércules, EE.UU) following the mixed molecular weight
254 (MW) protocol. After transfer, membranes were blocked with in-house tris-buffered saline, 0.1%
255 Tween20 and 5% milk (TBS-T 5%) for 90 min. Incubation with the primary antibody was kept at
256 4°C overnight. The primary antibodies used in this assay were: anti-SMAD3 (1:1000, Abcam,
257 40854), anti-p-SMAD3 (1:1000, Abcam, 63403), anti-SMAD2 (1:1000, Abcam, 40855), anti p-
258 SMAD2 (1:1000, Cell Signaling Technology, 3101).

259 Next day, incubation with secondary antibody was performed by 45min in TBST 5%, after
260 washed the membrane 3 times in TBST 5%. The secondary antibody used in this assay was goat
261 anti-rabbit IgG H&L (HRP) (Abcam, 205718) at 1:5000 for p-SMAD2 and p-SMAD3 and 1:15000
262 for SMAD2 and SMAD3. Finally, for protein visualization Clarity western ECL substrate (Biorad,
263 Hércules, EE.UU) was used and membranes were exposed in the ChemiDoc system (Biorad,
264 Hércules, EE.UU). Quantification of protein bands was carried on Image Lab software (Biorad,
265 Hércules, EE.UU) using the total protein standardisation method.

266 Western Blotting membranes were stripped and re-probed using Restore ™ PLUS Western Blot
267 Stripping Buffer (Thermo Fisher, Waltham, EE. UU) according to the manufacturer's protocol.
268 Incubation for 15 min in the buffer was followed by 3 washes with 1X TBS. Then, the membranes
269 were re-blocked and re-labelled following the previously described protocol.

270 Statistical analysis:

271 On one hand, mitochondrial activity, apoptosis, cell cycle, qPCR, Western Blot and wound
272 healing data visualization and statistical analysis were performed with the software GraphPad
273 Prism 8.00.

Mitochondrial activity was analysed using a linear regression model. Comparison of fluorescence increase with cell concentration did not show significant differences between both slopes ($\alpha = 0.05$). The apoptosis experiment results were analysed with 2ways-Anova to compare each different population between genotypes. A Sidak's multiple comparisons test was applied to correct the analysis. Finally, cell cycle results were analysed with a two-tailed unpaired t-test for each population (G2/M, S and G0/G1).

On the other hand, proteomic data analysis included different statistical analyses and data transformations along the pipeline. Initially, the data were normalised by variance stabilizing transformation (VSN). The data imputation for missing values was performed like missing not at random (MNAR) using the Minprob method with FDR < 0.01. Finally, differential expression analysis was performed using protein-wise linear models combined with empirical Bayes statistics implemented in the limma package, FDR < 0.05.

A third analysis was performed for the qPCR data. After normalization, fold changes (FC) were calculated concerning the geometric mean of the expression of each gene in the biological triplicates for *ALMS1* +/+ at 24h. Significant differences were calculates using a multiple t-test with a significant threshold of FDR < 0.05.

Finally western-blot data were normalized using total protein method following the methodology used by Clement et al. [22], [30] and as modified by Gürtler et al. [31]. After normalization FCs were calculated respect WT at 30 min of TGF-β1 stimulation. Significant differences were calculates using 2-way-ANOVA with a significant threshold of adj. p-value (FDR) < 0.05. For wound healing assay, a 2-way-ANOVA was applied and a significant threshold of adj. p-value (FDR) <0.05 was set.

RESULTS:

ALMS1 depletion does not alter mitochondrial basal activity despite generating G2/M cell cycle arrest in HeLa cells:

ALMS1 is a structural centromere protein [5] that controls the structure of the cytoskeleton [32]. Since *ALMS1* depletion causes cell cycle elongation [8], [33] it is expected that mitochondrial activity will also be altered, as both processes are dependent on each other and regulated by cytoskeletal dynamics. [34].

We evaluated the different phases of the cell cycle using the fox synchronous algorithm [35] to determine the Gaussian distribution of the different populations. DAPI fluorescence (461 nm)

305 and events count (cells) were displayed in the plots (Figure 1.A). After 24h of incubation, HeLa
306 cells ALMS1 -/- shown a significantly reduction (p-value < 0.05) in S phase from 24.26 % ± 1.32
307 in *ALMS1* +/+ to 19.27 % ± 1.69 in *ALMS1* -/-. The cell cycle arrest was caused by a significant
308 increase in the G2/M population (p-value < 0.01), from 1.6% ± 0.62 in *ALMS1* +/+ to 4.88 % ±
309 0.80 (Figure 1.B). The results in the G0/G1 population did not show significant differences
310 between genotypes. Despite this, the basal mitochondrial activity did not show a significant
311 difference between *ALMS1* +/+ and *ALMS1* -/- (Figure 1.C).

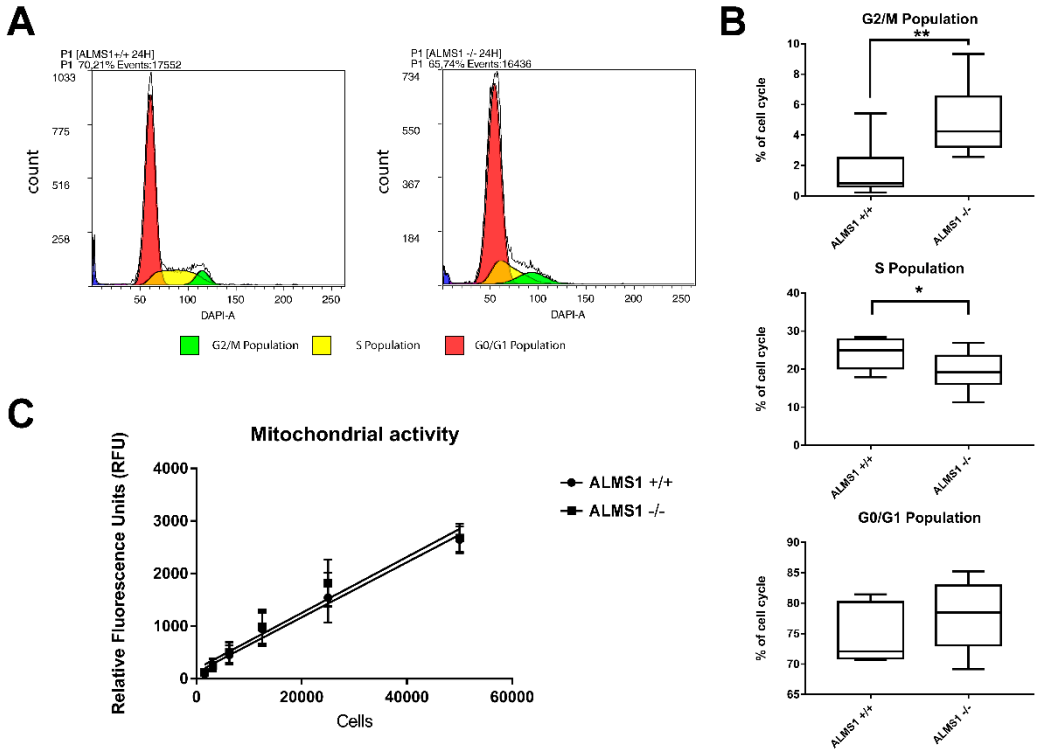

312

313 **Figure 1.** Cell cycle assay and mitochondrial activity results. **(A)** Cytometry plots with DAPI fluorescence and events
314 count. Colors correspond with each population defined by fox synchronous algorithm. **(B)** Box-plot for each
315 population previously defined in the cytometry plot that represents the percentage of cell cycle populations from
316 parent population. **(C)** Linear regression between relative fluorescence units (RFU) and cell concentration in both
317 genotypes (*ALMS1 +/+* and *ALMS1 -/-*). This experiment was carried out in triplicate and repeated 3 times on different
318 days (N=3, n=3). *: p-value < 0.05, **: p-value < 0.01.

319 The lack of *ALMS1* in HeLa prevents apoptosis induced by C2-ceramides
320 and Thapsigargin:

321 Accumulation of cells in G2/M phase triggers apoptosis by different pathways such as caspases
322 [36], [37]. We evaluated whether these cells were sensitive to apoptosis in response to an ER
323 stress-inducing stimulus (Thapsigargin; THAP) [38], and a pro-apoptotic sphingolipid such as C2-
324 ceramide.

As in the cell cycle assay, initial isolation of the cell population (P1) of interest was performed. Plots were represented with the FL4 (7-AAD) fluorescence in the y-axis and FL1 (Annexin V) fluorescence in the x-axis, both on a logarithmic scale. Thresholds for different populations (viable, early apoptotic, late apoptotic, and necrotic) were defined by a previous compensation analysis using THAP-like positive control of cell death. Finally, experiments were performed by triplicates in the plate (n=3) and in 3 alternative days (N=3).

Genotypes *ALMS1* +/+ and *ALMS1* -/- showed significant differences in viable (44.02% and 69.49%, respectively) and early apoptotic (43,47% and 23,44%) populations in cells stimulated with C2-C (Figure 2.A-B). Moreover, cells stimulated with THAP also showed significant differences between genotypes in viable (49,56% and 71,33%), early apoptotic (18,25% and 8,56%) and late apoptotic (25,09% and 11,93%) populations (Figure 2.C-D). These results indicate a resistance to apoptosis for these stimuli due to the lack of the *ALMS1*.

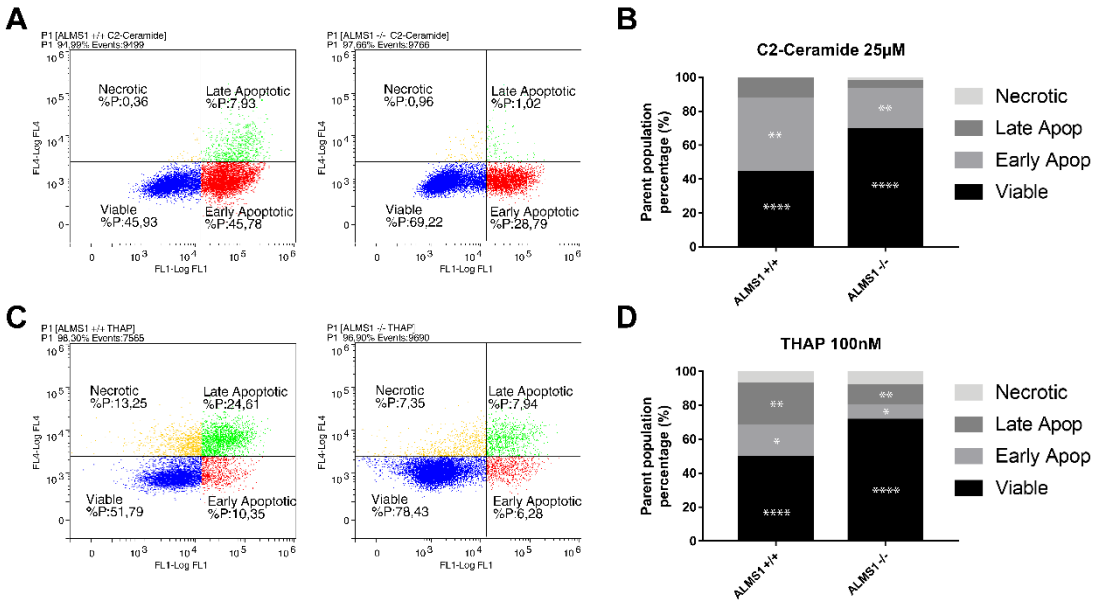

Figure 2. Apoptosis assay by annexin-V IP. **(A)** Cytometry plots for C2-ceramide (C2-C) with Log FL4 channel (IP) vs Log FL1 channel (Annexin-v). **(B)** Stacked-bar graph for cells treated with C2-C in a concentration of 25 µM. Percentages of each population are represented from a parent population previously defined. **(C)** Cytometry plots for thapsigargin (THAP) with Log FL4 channel (IP) vs Log FL1 channel (Annexin-v). **(D)** Stacked-bar graph for cells treated with THAP in a concentration of 100nM. Percentages of each population are represented from a parent population previously defined. This experiment was carried out in triplicate and repeated 3 times on different days (N=3, n=3). *: adj. p-value < 0.05, **: adj. p-value < 0.01, ***: adj. p-value < 0.001, ****: adj. p-value < 0.0001.

The proteomic profile in HeLa cells reveals *ALMS1* like a regulator of cell adhesion through the TGF-β pathway:

TGF-β is a pathway that plays a key role in the control of cell proliferation and apoptotic processes [14]. Since signal transduction through this pathway occurs via the primary cilium [13], [39], the lack of *ALMS1* could explain the aberrant processes seen above.

We evaluated how *ALMS1* depletion affects the signal transduction through stimulated TGF-β pathway. In this bulk analysis, we obtained a total of 86 differentially expressed proteins (DEP) (Figure 3.A), 31 (36%) over-expressed and 55 (64%) under-expressed. The variation in protein expression in this dataset can be explained mainly by a single principal component (Figure 3B). This would make sense as the main difference between these two genotypes would be the presence or absence of the *ALMS1* gene. From this dataset, a total of 76 proteins were associated with genes (Figure 3.C).

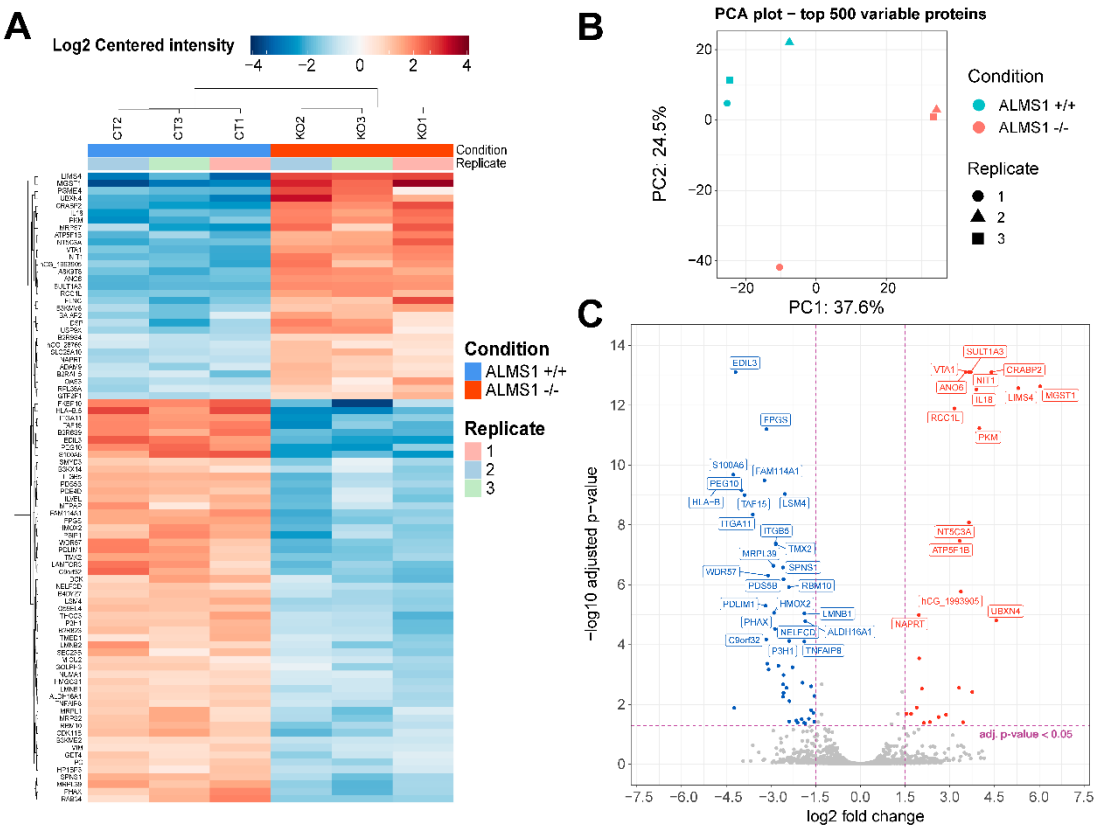

Figure 3. Differential expression analysis for proteomic data in HeLa. **(A)** Heatmap for all proteins (associated and not associated with genes) differentially expressed. Plot shows the expression pattern for the 3 biological replicates of genotype *ALMS1 +/+* (CT) and genotype *ALMS1 -/-* (KO). **(B)** Principal components analysis (PCA) for the top 500 variable proteins with all biological replicates for each genotype. **(C)** Volcano-plot showing the top 40 most significant genes associated with proteins. Proteins with no clear gene association were removed from this plot. Significant thresholds: log2 FC > 1.5, adj p-value < 0.05. This experiment was carried out in triplicate (n=3).

365 Based on the DE of protein-coding genes (PCG) we performed an enrichment analysis obtaining
366 a total of 9 GO terms significantly overrepresented (adj. p-value < 0.05) (Figure 4. A-B). The
367 majority of these PCG were associated with focal adhesion, cell-cell or cell-substrate
368 interactions. This result suggests the implication of *ALMS1* in the control of adhesion processes.
369 In addition, we calculated the z-score of these GO terms (Figure 4.A), showed a significant
370 decrease in process related to the ability of these cells to properly migrate or adhere to each
371 other or their matrix.

372 Moreover, genes such as vimentin (*VIM*) and desmoplakin (*DSP*), common biomarkers of EMT,
373 were associated with these GO terms (Figure 4.B). Interestingly, these genes exhibited an
374 expression pattern opposite to that observed when EMT process is activated.

375 Finally, *ITGB5* and *ITGA11*, two integrins whose activation plays an important role in the normal
376 development of EMT, proliferation and invasion are inhibited [40], [41].

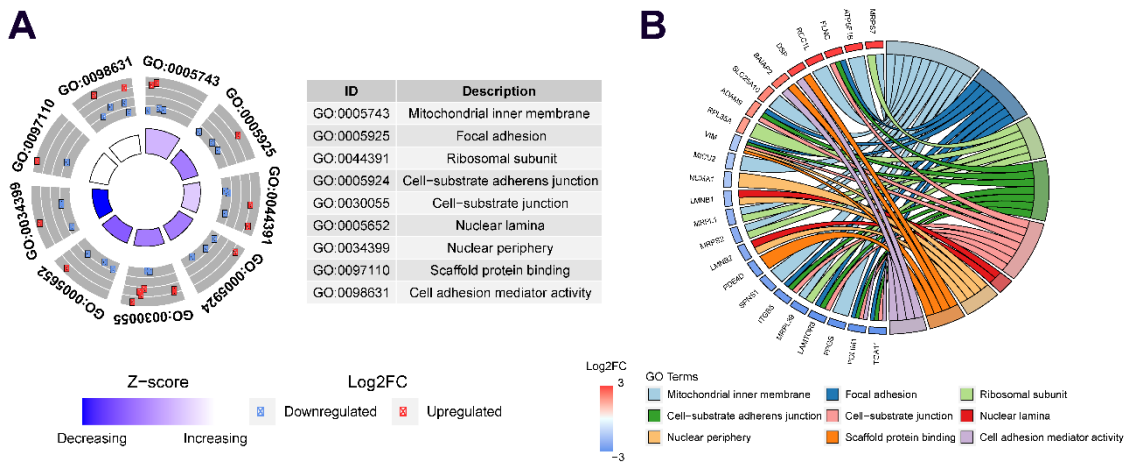

ID	Description
GO:0005743	Mitochondrial inner membrane
GO:0005925	Focal adhesion
GO:0044391	Ribosomal subunit
GO:0005924	Cell-substrate adherens junction
GO:0030055	Cell-substrate junction
GO:0005652	Nuclear lamina
GO:0034399	Nuclear periphery
GO:0097110	Scaffold protein binding
GO:0098631	Cell adhesion mediator activity

377

378 **Figure 4.** Enrichment analysis based on Go terms for proteomic data. **(A)** GoCircle-plot that includes significant over-
379 represented GoTerms in a table (ID and Name) and scatter plot with FC of any gene related with each GoTerm.
380 Moreover, this plot includes Z-score which is an estimation of up-regulation or down-regulation in the Goterm. **(B)**
381 Circus-Plot applied to Goterms to relate any Gene name with the corresponding GoTerm name. The plot also shows
382 the FC of each gene, and the list is sorted by FC from the most over-expressed (3) up to the most under-expressed (-
383 3).

384 *ALMS1* depletion alters the expression pattern of TGF-β1-induced EMT 385 markers in HeLa:

386 Proteomic analysis showed alterations in several adhesion processes coupled with aberrant
387 expression of EMT-related genes (*VIM*, *DSP*, *ITGB5* and *ITGA11*). We measure the main EMT
388 markers in our *ALMS1*-deficiency HeLa cells and compare it with another *ALMS1* model in the
389 hTERT-BJ-5ta line.

We evaluated the expression of the principal EMT biomarkers (*SNAI1*, *CDH2*, *TWIST1*, *ACTA2*, *VIM,* and *DSP*) and other genes related to EMT (*POSTN*, *EDIL3*). We perform stimulations at different time points (24, 48 and 72 h for HeLa and 24 and 48 h for BJ-5ta) with rh-TGF-β1 (2ng/mL) stimulation.

In HeLa (Figure 5.A) at 24 hours of stimulation *POSTN*, *SNAI1*, *VIM, ACTA2* and *EDIL3* were found under-expressed, while *TWIST1* and *DSP* were over-expressed. This data confirms the expression pattern previously detected in the proteome analysis related to the genes *VIM*, *DSP* and *EDIL3* (Figure 5.B). At 48 hours of stimulation, the over-expressed genes *CDH2*, *TWIST1* and *DSP*, in addition to *EDIL3* and *VIM* inhibition, showed significant differences (Figure 5.A). No other tested gene were significant. Finally, at 72 hours of stimulation the expression pattern was like the previous stimulation time points. However, the data dispersion was too high, and no significant differences were detected.

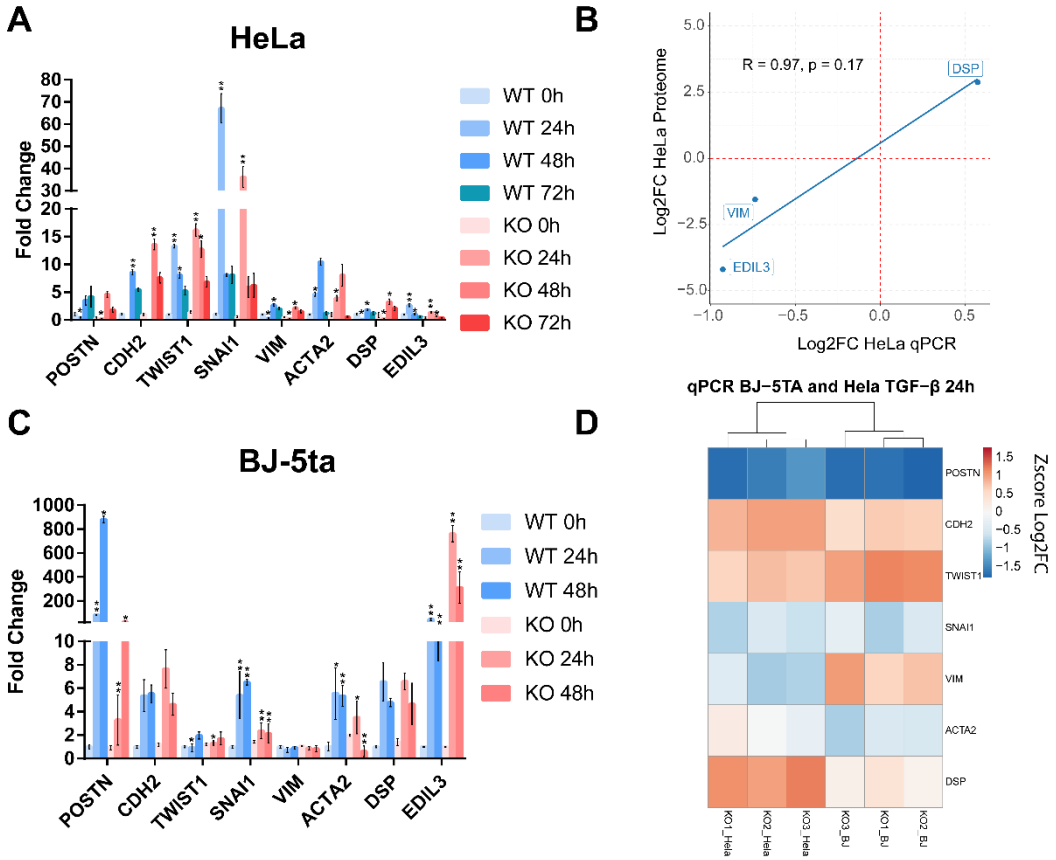

Figure 5. Expression measurement by qPCR of different EMT biomarkers with TGF-β stimulation at **(A)** 0, 24, 48, and 72 hours in HeLa. **(B)** Correlation plot between the expression of three EMT markers in the HeLa proteomic analysis and the HeLa qPCR assay. The expression is represented based on the log2 FC and the R coefficient using Pearson's method. **(C)** Expression measurement of EMT markers by qPCR in BJ-5ta after 0, 24 and 48 hours of stimulation with TGF-β1 ligand **(D)** Comparative heatmap with Z-score values per sample of EMT markers in HeLa and BJ-5ta after 24

408 hours of TGF-β1 stimulation. These experiments were performed by triplicate (n=3). *: adj. p-value < 0.05, **: adj. p-
409 value < 0.01.

410 In BJ-5ta (Figure 5.B) no inhibition of *VIM* or overexpression of *DSP* were detected. However,
411 inhibition of *POSTN* and the transcription factor (TF) *SNAI1* was constant in both cell lines as well
412 as the overexpression of *TWIST1*. *ACTA2* also showed decreased levels in HeLa but not as
413 significant as in BJ-5ta. After Z score normalization of log2FC both cell lines showed a similar
414 expression pattern of these markers (Figure 5C). EDIL3 is not shown in the heatmap as FC is too
415 high, so it could mask the differences of the rest of the markers.

416 Absence of *ALMS1* decreases migration capacity in HeLa and BJ-5ta and 417 reduce SMAD3 phosphorylation in BJ-5ta:

418 We evaluated the canonical activation of the TGF-β pathway. SMAD2 and SMAD3
419 phosphorilation levels were analysed at 4 different times (0, 10, 30 and 90 min) in BJ-5ta and 2
420 different times (0 and 30 min) in HeLa after TGF-β1 stimuli. The data shown that the lack of
421 *ALMS1* inhibits SMAD3 (Ser213) activation after 30min of TGF-β1 ligand exposure (p-value
422 <0.01) but not affects to SMAD2 phosphorylation in BJ-5ta (Figure 6 A-D). In HeLa cells no
423 alterations in canonical pathway signalling of TGF-β were detected (Figure 6 E, F). The p-
424 SMADs/SMADs ratios did not differ from the p-SMADs/total protein ratios, data not shown.

425 Finally, we measured cell migration capacity in both cell lines in the presence and absence of -
426 rh-TGF-β1 ligand. (Figure 6 G, H). *ALMS1* depletion reduced migration capacity compared to the
427 control line in both cell lines. This reduction is exacerbated after TGF-β stimulation in BJ-5ta
428 while in HeLa the tendency is the same in the presence or absence of the stimulus.

429

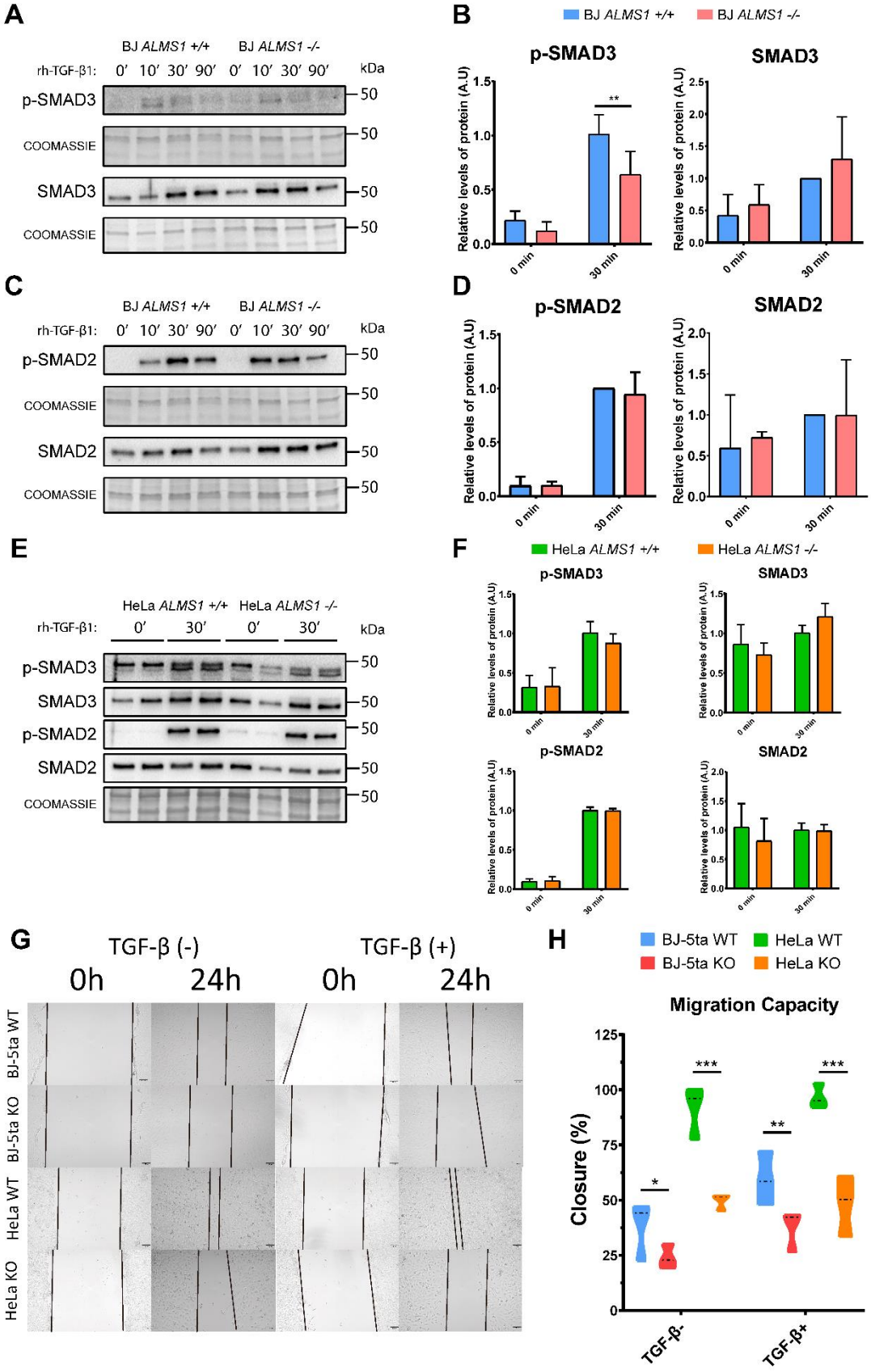

430

431 **Figure 6.** TGF-β canonical pathway activation assay and measurement of cell migration capacity in HeLa and BJ-5ta.

432 **(A)** Representative western-blot of p-SMAD3 and SMAD3 levels after 0, 10, 30 and 90 min of stimulation with TGF-β1

433 (2 ng/µL) ligand and their corresponding loading controls (coomassie). **(B)** Quantification of band intensity in WB for
434 p-SMAD3 and SMAD3 at time 0 and after 30 min stimulation with TGF-β1. (n=3). *: p-value < 0.05, **: p-value < 0.01
435 **(C)** Representative western-blot of p-SMAD2 and SMAD2 levels after 0, 10, 30 and 90 min of stimulation with TGF-β1
436 (2 ng/µL) ligand and their corresponding loading controls (coomassie). **(D)** Quantification of band intensity in WB for
437 p-SMAD2 and SMAD2 at time 0 and after 30 min stimulation with TGF-β1. (n=3). *: p-value < 0.05, **: p-value < 0.01.
438 **(E)** Representative western-blot of p-SMAD3, SMAD3, p-SMAD2 and SMAD2 levels after 0 and 30 min of stimulation
439 with TGF-β1 (2 ng/µL) ligand and their corresponding loading control (coomassie). **(F)** Quantification of band intensity
440 in WB for p-SMAD3, SMAD3, p-SMAD2 and SMAD2 at time 0 and after 30 min stimulation with TGF-β1. (n=2). *: p-
441 value < 0.05, **: p-value < 0.01 **(E)** Representative images of wound healing assay in HeLa (WT and KO) and BJ-5ta
442 (WT and KO) at 0 and24 hours in absence or presence of 2 ng/µL TGF-β1. **(F)** Quantification of the cell area of the
443 image and how it decreased after 24 hours of incubation (n=3). *: p-value < 0.05, **: p-value < 0.01, ***: p-value <
444 0.001.

445 # DISCUSSION:

446 In this study, we obtain similar results as previously described for the ALMS1 deficiency such as
447 cell cycle arrest [33] or resistance to apoptosis [8] in a new cell type. Moreover, we reported
448 new insights to understand the role of *ALMS1* in cell function and TGF-β signalling

449 Cell cycle arrest in the G2/M phase (Figure 1. A-B), also described in *ALMS1*-knockdown
450 cardiomyocytes [33], seems to be a cell process triggered by *ALMS1* depletion. Several studies
451 have already linked cell cycle arrest in the G2/M phase to the TGF-β pathway and the
452 development of fibrosis [42]–[44].

453 Normally, cell cycle arrest in both the G2/M and G0/G1 phases is often accompanied by the
454 activation of apoptotic processes [34], [45]–[47]. In contrast, depletion of *ALMS1* seems to
455 generate apoptosis resistance against THAP and C2-C in HeLa cells (Figure 2), which is in
456 accordance with that reported by Zulato et al., [8] in patient fibroblasts. THAP is a non-
457 competitive inhibitor for Ca^{2+}-ATPases located in the endoplasmic reticulum (SERCA). This,
458 inhibits Ca^{2+} reflux to the lumen of the endoplasmic reticulum, generating endoplasmic
459 reticulum stress (ER stress) [48]. At the same time, ER stress activates a signalling network called
460 Unfolded Protein Response (UPR) which alleviates this stress and promotes cell survival,
461 restoring ER homeostasis [49]. At this point, *ALMS1* depletion could be acting at two levels:
462 inhibiting THAP action (ER stress) or over-activating UPR and generating apoptosis resistance.
463 Because of the role of *ALMS1* in the centrosome and its relation with endocytic trafficking [32],
464 its depletion could probably alter the structure of the membrane, inhibiting the signalling
465 transduction of ligands like THAP. THAP also induces apoptosis impairing cytoskeleton dynamics
466 and disorganization of F-actin via mTORC1 inhibition in the mTORC1-RhoA-Limk-Cofilin-1 axis in
467 A549 cells [50]. *ALMS1* depletion already causes disorganization of the F-actin cytoskeleton [32]

468 but does not lead to cell death. Probably, the mTOR pathway through mTORC1 was inhibited in
469 *ALMS1* -/- cells, but in this case, other mechanisms could prevent cells from reaching apoptotic
470 stages. This would be supported by the inhibition of LAMTOR3 (Figure 4.B), a protein involved
471 in the formation of the Ragulator complex that activates mTORC1 [51].

472 C2-C is a sphingolipid that induces caspases-dependent apoptosis, inhibiting PI3K/AKT pathway
473 and increasing the depolarisation of the mitochondrial membrane [52]–[54]. The over-activation
474 of the PI3K/AKT pathway could explain the apoptotic resistance in the case of the C2-C [55], [56].
475 This fact would agree with the previous proposed mTORC1 inhibition, since phosphorylation of
476 AKT/PKB at s473 leads to inhibition of mTORC1 mediated by FoxO transcription factors [57],
477 which could be related to F-actin filament disorganisation previously described in Alström
478 fibroblasts [32].

479 In addition to the role of *ALMS1* in G2/M phase cell cycle arrest and resistance to THAP- and C2-
480 C-mediated apoptosis, this study suggests that *ALMS1* depletion leads to inhibition of TGF-β
481 signalling pathway. This could be affecting downstream processes such as cell migration and
482 adhesion.

483 After TGF-β stimulation, the lack of *ALMS1* alters the expression of several genes related to focal
484 adhesion and cell-substrate adherens junction (Figure 4 A-B), two processes required for TGF-
485 β1-induced EMT [58], [59]. This fact could be conditioning the activation of EMT, preventing cells
486 from moving into a mesenchymal state characterised by an increased migratory capacity.
487 Previous studies have demonstrated the relationship between signalling through the primary
488 cilium and the EMT focusing mainly on signalling through the WNT and SHH pathway in various
489 organs such as epicardial tissue, kidney epithelial cells, and pancreatic β-cells [31]–[34].
490 However, signalling through the TGF-β pathway has not yet been extensively studied in this
491 context.

492 Moreover, we have found interesting candidates in the HeLa proteome profiling that could
493 explain or be related to the mentioned cellular disturbances (Figure 3C). *S100A6*, under-
494 expressed, is a positive regulator of proliferation, migration and angiogenesis [60]–[62], and also
495 a regulator of endothelial calcium signalling [63]. *PKM*, which was over-expressed in HeLa cells,
496 is associated with apoptosis resistance [64]. *ITGA11*, another gene under-expressed in this cell
497 line and related to fibrosis generation, is expressed due to activation of the TGF-β pathway [65].
498 Finally, two known EMT markers, *VIM* and *DSP*, showed a reverse pattern to that expected when
499 this process is activated. *VIM* is a key player in the regulation of EMT and its deficiency leads to
500 inhibition of this process [66]. On the other hand, *DSP* is a protein involved in cell-cell junctions

501 mediated by desmosomes. It is therefore considered a typical epithelial marker whose decrease
502 is related to the passage of the cell from an epithelial to a mesenchymal state [67]. This could
503 be first evidence suggesting inhibition of the TGF-β1-induced EMT when *ALMS1* is missing.

504 One of the most relevant detected genes was *SNAI1,* which is inhibited in both cell lines (HeLa
505 and BJ-5ta). *SNAI1* and *TWIST1* are transcription factors that repress E-cadherin (*CDH1*)
506 expression and activate the expression of N-cadherins (*CDH2*) [68], [69]. E/N-cadherins switch is
507 involved in the induction of EMT [70], [71] through the TGF-β pathway [72]. Inhibition of *SNAI1*
508 could be affecting the normal EMT in these cells. The decreased expression of *SNAI1,* together
509 with the inhibition of *ACTA2* and *POSTN,* also suggests that TGF-β1-induced EMT would be
510 down-regulated. *SNAI1* is up-regulated by SMAD3, which is phosphorylated when the TGF-β
511 pathway is activated and forms a complex with SMAD2 [17]. The phosphorylated SMAD2-
512 SMAD3 complex translocates to the nucleus, activating the expression of several genes related
513 to cell migration and EMT such as *SNAI1* [73]. Because we detected consistent inhibition in both
514 cell models of *SNAI1*, we sought to determine whether SMAD3 and SMAD2 activation was also
515 compromised in BJ-5ta and HeLa models. In BJ-5ta, we conclude that *ALMS1* depletion inhibits
516 SMAD3 phosphorylation but not affect SMAD2 phosphorylation (Figure 6 A-D). This fact could
517 lead to downstream inhibition of *SNAI1* and affect migration and adhesion capacity in this cell
518 line (Figure 6 G, H). In HeLa, no alterations in the activation of the canonical TGF-β pathway were
519 detected (Figure 6 E, F). In addition, a decrease in cell migration capacity was observed, but
520 independently of TGF-β, in contrast to BJ-5ta (Figure 6 G, H). This could explain that the
521 involvement of ALMS1 in cell migration is a conserved process, but its regulation is a cell type-
522 dependent process.

523 We have previously described that *ALMS1* depletion by siRNA inhibits SMAD2 phosphorylation
524 in the hTERT RPE-1 cell line [10] but this was not detected in any of our KO models. The only
525 alteration detected in the canonical pathway was the inhibition of SMAD3 activation in BJ-5ta.
526 This difference could be due to the cell type or to differences between the KO and siRNA models.

527 This facts leads us to hypothesise that inhibition of p-SMAD3 could prevent the formation of the
528 SMAD2/3 complex, affecting the expression of *SNAI1* in BJ-5ta. [20]. Whereas in HeLa, inhibition
529 of *SNAI1* and cell migration capacity appears to involve other regulatory mechanisms.

530

CONCLUSION:

ALMS1 appears to have a role in the regulation of cell cycle and apoptotic processes but does not affect mitochondrial reduction capacity in HeLa. *ALMS1* depletion affects signal transduction through the TGF-β pathway, altering the expression of several EMT-related genes in BJ-5ta and HeLa. However, the canonical (SMAD-dependent) pathway did not show major differences. Finally downstream processes such as cell migration and adhesion capacity appear to be compromised in the absence of *ALMS1*.

Author Contributions: BB-M and DV designed the study. BB-M performed the experiments and analysed the data. EN-G assisted in performing apoptosis, cell cycle and mitochondrial activity assays. AI-R assisted in the quantification of the expression of EMT markers in the BJ-5ta model and in the cell migration assay. BB-M and DV wrote the manuscript. All authors have read the draft and provided approval for publication.

Data Availability Statement: Proteomic data are available via ProteomeXchange with identifier PXD024964.

Acknowledgments: We sincerely thank the Proteomics and Genomics services from Centro de Apoyo Científico-Tecnológico a la Investigación (CACTI) of University of Vigo and its specialists Paula Álvarez Chaver, Ángel Sebastián Comesaña, Verónica Outeiriño and Manuel Marcos for their guidance and advise. We also thank Mercedes Peleteiro Olmedo from Centro de Investigacións Biomédicas (CINBIO) from University of Vigo for the flow cytometry service.

Funding: This work was funded by Instituto de Salud Carlos III (project PI15/00049 and PI19/00332), Xunta de Galicia (Centro de Investigación de Galicia CINBIO 2019-2022; Ref. ED431G-2019/06) and Consolidación e estructuración de unidades de investigación competitivas e outras accións de fomento (Xunta de Galicia, ED431C-2018/54). Brais Bea-Mascato (FPU17/01567) was supported by graduate studentship awards (FPU predoctoral fellowship) from the Spanish Ministry of Education, Culture and Sports.

Conflicts of Interest: The authors declare no conflict of interest. The funders had no role in the design of the study; in the collection, analyses, or interpretation of data; in the writing of the manuscript, or in the decision to publish the results.

BIBLIOGRAPHY:

[1] J. D. Marshall, P. Maffei, G. B. Collin, and J. K. Naggert, “Alström syndrome: genetics and clinical overview,” *Curr. Genomics*, vol. 12, no. 3, pp. 225–235, May 2011, doi: 10.2174/138920211795677912.

[2] A. B. Jaykumar, P. Caceres, E. L. Henson, W. H. Beierwaltes, and P. A. Ortiz, “Deletion of ALMS1 (Alstrom Syndrome 1) enhances salt-sensitive hypertension, and induces insulin resistance and obesity in rats.,” *FASEB J.*, vol. 31, no. 1_supplement, pp. 857.26-857.26, Apr. 2017, doi: 10.1096/fasebj.31.1_supplement.857.26.

[3] G. B. Collin *et al.*, “Mutations in ALMS1 cause obesity, type 2 diabetes and neurosensory degeneration in Alström syndrome,” *Nat. Genet.*, vol. 31, p. 74, Apr. 2002, [Online]. Available: https://doi.org/10.1038/ng867.

[4] J. D. Marshall *et al.*, “Spectrum of ALMS1 variants and evaluation of genotype-phenotype correlations in Alström syndrome,” *Hum. Mutat.*, vol. 28, no. 11, pp. 1114–1123, Nov. 2007, doi: 10.1002/humu.20577.

[5] T. Hearn *et al.*, “Subcellular Localization of ALMS1 Supports Involvement of Centrosome and Basal Body Dysfunction in the Pathogenesis of Obesity, Insulin Resistance, and Type 2 Diabetes,” *Diabetes*, vol. 54, no. 5, pp. 1581 LP – 1587, May 2005, doi: 10.2337/diabetes.54.5.1581.

[6] D. Jagger *et al.*, “Alström Syndrome protein ALMS1 localizes to basal bodies of cochlear hair cells and regulates cilium-dependent planar cell polarity.,” *Hum. Mol. Genet.*, vol. 20, no. 3, pp. 466–481, Feb. 2011, doi: 10.1093/hmg/ddq493.

[7] G. Li *et al.*, “A role for Alström syndrome protein, alms1, in kidney ciliogenesis and cellular quiescence,” *PLoS Genet.*, vol. 3, no. 1, pp. e8–e8, Jan. 2007, doi: 10.1371/journal.pgen.0030008.

[8] E. Zulato *et al.*, “ALMS1-deficient fibroblasts over-express extra-cellular matrix components, display cell cycle delay and are resistant to apoptosis,” *PLoS One*, vol. 6, no. 4, pp. e19081–e19081, Apr. 2011, doi: 10.1371/journal.pone.0019081.

[9] C. C. Leitch, S. Lodh, V. Prieto-Echagüe, J. L. Badano, and N. A. Zaghloul, “Basal body proteins regulate Notch signaling through endosomal trafficking.,” *J. Cell Sci.*, vol. 127, no. Pt 11, pp. 2407–2419, Jun. 2014, doi: 10.1242/jcs.130344.

590 [10] M. Álvarez-Satta *et al.*, “ALMS1 Regulates TGF-β Signaling and Morphology of Primary
591 Cilia,” *Frontiers in Cell and Developmental Biology*, vol. 9, p. 112, 2021.

592 [11] A. B. Roberts *et al.*, “Smad3 is key to TGF-β-mediated epithelial-to-mesenchymal
593 transition, fibrosis, tumor suppression and metastasis,” *Cytokine Growth Factor Rev.*,
594 vol. 17, no. 1–2, pp. 19–27, Feb. 2006, doi: 10.1016/J.CYTOGFR.2005.09.008.

595 [12] W. KL, J. KE, and H. CA, “Targeting TGF-β Mediated SMAD Signaling for the Prevention
596 of Fibrosis,” *Front. Pharmacol.*, vol. 8, no. JUL, Jul. 2017, doi:
597 10.3389/FPHAR.2017.00461.

598 [13] C. A. Clement *et al.*, “TGF-β Signaling Is Associated with Endocytosis at the Pocket
599 Region of the Primary Cilium,” *Cell Rep.*, vol. 3, no. 6, pp. 1806–1814, 2013, doi:
600 https://doi.org/10.1016/j.celrep.2013.05.020.

601 [14] Y. Zhang, P. B. Alexander, and X. F. Wang, “TGF-β family signaling in the control of cell
602 proliferation and survival,” *Cold Spring Harb. Perspect. Biol.*, vol. 9, no. 4, Apr. 2017, doi:
603 10.1101/cshperspect.a022145.

604 [15] L. K, “Signaling Cross Talk between TGF-β/Smad and Other Signaling Pathways,” *Cold*
605 *Spring Harb. Perspect. Biol.*, vol. 9, no. 1, Jan. 2017, doi:
606 10.1101/CSHPERSPECT.A022137.

607 [16] J. Massagué, “TGFβ signalling in context,” *Nature Reviews Molecular Cell Biology*, vol.
608 13, no. 10. NIH Public Access, pp. 616–630, Oct. 2012, doi: 10.1038/nrm3434.

609 [17] A. Nakao *et al.*, “TGF-β receptor-mediated signalling through Smad2, Smad3 and
610 Smad4,” *EMBO J.*, vol. 16, no. 17, pp. 5353–5362, Sep. 1997, doi:
611 10.1093/EMBOJ/16.17.5353.

612 [18] S. Thuault, E.-J. Tan, H. Peinado, A. Cano, C.-H. Heldin, and A. Moustakas, “HMGA2 and
613 Smads Co-regulate SNAIL1 Expression during Induction of Epithelial-to-Mesenchymal
614 Transition,” *J. Biol. Chem.*, vol. 283, no. 48, p. 33437, Nov. 2008, doi:
615 10.1074/JBC.M802016200.

616 [19] Y. Wang, J. Shi, K. Chai, X. Ying, and B. P. Zhou, “The Role of Snail in EMT and
617 Tumorigenesis.”

618 [20] T. Vincent *et al.*, “A SNAIL1-SMAD3/4 transcriptional repressor complex promotes TGF-
619 β mediated epithelial-mesenchymal transition,” *Nat. Cell Biol.*, vol. 11, no. 8, pp. 943–
620 950, 2009, doi: 10.1038/ncb1905.

621 [21] X. Yan *et al.*, “Smad7 Protein Interacts with Receptor-regulated Smads (R-Smads) to
622 Inhibit Transforming Growth Factor-β (TGF-β)/Smad Signaling *,” *J. Biol. Chem.*, vol.
623 291, no. 1, pp. 382–392, Jan. 2016, doi: 10.1074/JBC.M115.694281.

624 [22] M. Mönnich *et al.*, “CEP128 Localizes to the Subdistal Appendages of the Mother
625 Centriole and Regulates TGF-β/BMP Signaling at the Primary Cilium,” *Cell Rep.*, vol. 22,
626 no. 10, pp. 2584–2592, Mar. 2018, doi: 10.1016/J.CELREP.2018.02.043.

627 [23] N. E. Sanjana, O. Shalem, and F. Zhang, “Improved vectors and genome-wide libraries
628 for CRISPR screening,” *Nat. Methods*, vol. 11, no. 8, pp. 783–784, 2014, doi:
629 10.1038/nmeth.3047.

630 [24] X. Zhang, A. H. Smits, G. B. van Tilburg, H. Ovaa, W. Huber, and M. Vermeulen,
631 “Proteome-wide identification of ubiquitin interactions using UbIA-MS.,” *Nat. Protoc.*,
632 vol. 13, no. 3, pp. 530–550, Mar. 2018, doi: 10.1038/nprot.2017.147.

633 [25] G. Yu, L.-G. Wang, Y. Han, and Q.-Y. He, “clusterProfiler: an R package for comparing
634 biological themes among gene clusters,” *OMICS*, vol. 16, no. 5, pp. 284–287, May 2012,
635 doi: 10.1089/omi.2011.0118.

636 [26] W. Walter, F. Sánchez-Cabo, and M. Ricote, “GOplot: an R package for visually
637 combining expression data with functional analysis.,” *Bioinformatics*, vol. 31, no. 17,
638 pp. 2912–2914, Sep. 2015, doi: 10.1093/bioinformatics/btv300.

639 [27] Y. Perez-Riverol *et al.*, “The PRIDE database and related tools and resources in 2019:
640 improving support for quantification data.,” *Nucleic Acids Res.*, vol. 47, no. D1, pp.
641 D442–D450, Jan. 2019, doi: 10.1093/nar/gky1106.

642 [28] C. A. Schneider, W. S. Rasband, and K. W. Eliceiri, “NIH Image to ImageJ: 25 years of
643 image analysis,” *Nat. Methods 2012 97*, vol. 9, no. 7, pp. 671–675, Jun. 2012, doi:
644 10.1038/nmeth.2089.

645 [29] A. Suarez-Arnedo, F. T. Figueroa, C. Clavijo, P. Arbeláez, J. C. Cruz, and C. Muñoz-
646 Camargo, “An image J plugin for the high throughput image analysis of in vitro scratch
647 wound healing assays,” *PLoS One*, vol. 15, no. 7, Jul. 2020, doi:
648 10.1371/JOURNAL.PONE.0232565.

649 [30] C. A. Clement *et al.*, “TGF-β Signaling Is Associated with Endocytosis at the Pocket
650 Region of the Primary Cilium,” *Cell Rep.*, vol. 3, no. 6, pp. 1806–1814, Mar. 2013, doi:
651 10.1016/j.celrep.2013.05.020.

652 [31] A. Gürtler *et al.*, “Stain-Free technology as a normalization tool in Western blot
653 analysis,” *Anal. Biochem.*, vol. 433, no. 2, pp. 105–111, Feb. 2013, doi:
654 10.1016/J.AB.2012.10.010.

655 [32] G. B. Collin *et al.*, “The Alström syndrome protein, ALMS1, interacts with α-actinin and
656 components of the endosome recycling pathway,” *PLoS One*, vol. 7, no. 5, pp. e37925–
657 e37925, 2012, doi: 10.1371/journal.pone.0037925.

658 [33] L. T. Shenje *et al.*, “Mutations in Alström protein impair terminal differentiation of
659 cardiomyocytes,” *Nat. Commun.*, vol. 5, p. 3416, Mar. 2014, doi: 10.1038/ncomms4416.

660 [34] R. Horbay and R. Bilyy, “Mitochondrial dynamics during cell cycling,” *Apoptosis*, vol. 21,
661 no. 12. Springer New York LLC, pp. 1327–1335, Dec. 01, 2016, doi: 10.1007/s10495-016-
662 1295-5.

663 [35] M. H. Fox, “A model for the computer analysis of synchronous DNA distributions
664 obtained by flow cytometry.,” *Cytometry*, vol. 1, no. 1, pp. 71–77, Jul. 1980, doi:
665 10.1002/cyto.990010114.

666 [36] L. M. Westrate, A. D. Sayfie, D. M. Burgenske, and J. P. MacKeigan, “Persistent
667 mitochondrial hyperfusion promotes G2/M accumulation and caspase-dependent cell
668 death,” *PLoS One*, vol. 9, no. 3, p. 91911, Mar. 2014, doi:
669 10.1371/journal.pone.0091911.

670 [37] D. Arita, M. Kambe, C. Ishioka, and R. Kanamaru, “Induction of p53-independent
671 apoptosis associated with G2M arrest following DNA damage in human colon cancer
672 cell lines,” *Japanese J. Cancer Res.*, vol. 88, no. 1, pp. 39–43, Jan. 1997, doi:
673 10.1111/j.1349-7006.1997.tb00299.x.

674 [38] I. Yoshida, A. Monji, K. Tashiro, K. Nakamura, R. Inoue, and S. Kanba, “Depletion of
675 intracellular Ca2+ store itself may be a major factor in thapsigargin-induced ER stress
676 and apoptosis in PC12 cells,” *Neurochem. Int.*, vol. 48, no. 8, pp. 696–702, 2006, doi:
677 https://doi.org/10.1016/j.neuint.2005.12.012.

678 [39] S. T. Christensen, S. K. Morthorst, J. B. Mogensen, and L. B. Pedersen, “Primary cilia and
679 coordination of receptor tyrosine kinase (RTK) and transforming growth factor β (TGF-
680 β) signaling,” *Cold Spring Harbor Perspectives in Biology*, vol. 9, no. 6. Cold Spring
681 Harbor Laboratory Press, p. a028167, Jun. 01, 2017, doi: 10.1101/cshperspect.a028167.

682 [40] A. Bianchi, M. E. Gervasi, and A. Bakin, “Role of β5-integrin in epithelial-mesenchymal

683 transition in response to TGF-β," *Cell Cycle*, vol. 9, no. 8, pp. 1647–1659, Apr. 2010, doi:
684 10.4161/cc.9.8.11517.

685 [41] P. Erusappan, J. Alam, N. Lu, C. Zeltz, and D. Gullberg, "Integrin α11 cytoplasmic tail is
686 required for FAK activation to initiate 3D cell invasion and ERK-mediated cell
687 proliferation.," *Sci. Rep.*, vol. 9, no. 1, p. 15283, Oct. 2019, doi: 10.1038/s41598-019-
688 51689-6.

689 [42] L. Yang, T. Y. Besschetnova, C. R. Brooks, J. V Shah, and J. V Bonventre, "Epithelial cell
690 cycle arrest in G2/M mediates kidney fibrosis after injury," *Nat. Med.*, vol. 16, no. 5, pp.
691 535–543, 2010, doi: 10.1038/nm.2144.

692 [43] T. L. White, N. Deshpande, V. Kumar, A. G. Gauthier, and U. V Jurkunas, "Cell cycle re-
693 entry and arrest in G2/M phase induces senescence and fibrosis in Fuchs Endothelial
694 Corneal Dystrophy.," *Free Radic. Biol. Med.*, vol. 164, pp. 34–43, Feb. 2021, doi:
695 10.1016/j.freeradbiomed.2020.12.445.

696 [44] H. Li *et al.*, "Atg5-mediated autophagy deficiency in proximal tubules promotes cell
697 cycle G2/M arrest and renal fibrosis.," *Autophagy*, vol. 12, no. 9, pp. 1472–1486, Sep.
698 2016, doi: 10.1080/15548627.2016.1190071.

699 [45] J. JAKUBIKOVA, Y. BAO, and J. SEDLAK, "Isothiocyanates Induce Cell Cycle Arrest,
700 Apoptosis and Mitochondrial Potential Depolarization in HL-60 and Multidrug-resistant
701 Cell Lines," *Anticancer Res.*, vol. 25, no. 5, 2005.

702 [46] N. B. Madungwe *et al.*, "Mitochondrial inner membrane protein (Mitofilin) knockdown
703 induces cell death by apoptosis via an AIF-PARP-dependent mechanism and cell cycle
704 arrest," *Am. J. Physiol. - Cell Physiol.*, vol. 315, no. 1, pp. C28–C43, Jul. 2018, doi:
705 10.1152/ajpcell.00230.2017.

706 [47] Y. Liu *et al.*, "Calycosin induces mitochondrial-dependent apoptosis and cell cycle
707 arrest, and inhibits cell migration through a ROS-mediated signaling pathway in HepG2
708 hepatocellular carcinoma cells," *Toxicol. Vitr.*, vol. 70, p. 105052, Feb. 2021, doi:
709 10.1016/j.tiv.2020.105052.

710 [48] P. Lindner, S. B. Christensen, P. Nissen, J. V. Møller, and N. Engedal, "Cell death induced
711 by the ER stressor thapsigargin involves death receptor 5, a non-autophagic function of
712 MAP1LC3B, and distinct contributions from unfolded protein response components,"
713 *Cell Commun. Signal.*, vol. 18, no. 1, p. 12, 2020, doi: 10.1186/s12964-019-0499-z.

714 [49] C. M. Oslowski and F. Urano, “Measuring ER stress and the unfolded protein response
715 using mammalian tissue culture system,” *Methods Enzymol.*, vol. 490, pp. 71–92, 2011,
716 doi: 10.1016/B978-0-12-385114-7.00004-0.

717 [50] F. Wang *et al.*, “Thapsigargin Induces Apoptosis by Impairing Cytoskeleton Dynamics in
718 Human Lung Adenocarcinoma Cells,” *Sci. World J.*, vol. 2014, p. 619050, 2014, doi:
719 10.1155/2014/619050.

720 [51] Z. Mu, L. Wang, W. Deng, J. Wang, and G. Wu, “Structural insight into the Ragulator
721 complex which anchors mTORC1 to the lysosomal membrane,” *Cell Discov.*, vol. 3, no.
722 1, p. 17049, 2017, doi: 10.1038/celldisc.2017.49.

723 [52] M. J. Zinda, C. J. Vlahos, and M. T. Lai, “Ceramide Induces the Dephosphorylation and
724 Inhibition of Constitutively Activated Akt in PTEN Negative U87MG Cells,” *Biochem.*
725 *Biophys. Res. Commun.*, vol. 280, no. 4, pp. 1107–1115, 2001, doi:
726 https://doi.org/10.1006/bbrc.2000.4248.

727 [53] R. M. Sánchez-Mora, H. Arboleda, and G. Arboleda, “PINK1 Overexpression Protects
728 Against C2-ceramide-Induced CAD Cell Death Through the PI3K/AKT Pathway,” *J. Mol.*
729 *Neurosci.*, vol. 47, no. 3, pp. 582–594, 2012, doi: 10.1007/s12031-011-9687-z.

730 [54] A. S. Arora, B. J. Jones, T. C. Patel, S. F. Bronk, and G. J. Gores, “Ceramide induces
731 hepatocyte cell death through disruption of mitochondrial function in the rat,”
732 *Hepatology*, vol. 25, no. 4, pp. 958–963, Apr. 1997, doi:
733 https://doi.org/10.1002/hep.510250428.

734 [55] S.-J. Jeong *et al.*, “PI3K/AKT inhibition induces caspase-dependent apoptosis in HTLV-1-
735 transformed cells,” *Virology*, vol. 370, no. 2, pp. 264–272, 2008, doi:
736 https://doi.org/10.1016/j.virol.2007.09.003.

737 [56] B. N. Fahy, M. Schlieman, S. Virudachalam, and R. J. Bold, “AKT inhibition is associated
738 with chemosensitisation in the pancreatic cancer cell line MIA-PaCa-2,” *Br. J. Cancer*,
739 vol. 89, no. 2, pp. 391–397, 2003, doi: 10.1038/sj.bjc.6601037.

740 [57] C.-C. Chen *et al.*, “FoxOs Inhibit mTORC1 and Activate Akt by Inducing the Expression of
741 Sestrin3 and Rictor,” *Dev. Cell*, vol. 18, no. 4, pp. 592–604, 2010, doi:
742 https://doi.org/10.1016/j.devcel.2010.03.008.

743 [58] C. Cicchini *et al.*, “TGFβ-induced EMT requires focal adhesion kinase (FAK) signaling,”
744 *Exp. Cell Res.*, vol. 314, no. 1, pp. 143–152, 2008, doi:

745 https://doi.org/10.1016/j.yexcr.2007.09.005.

746 [59] T. Baronsky *et al.*, “Cell-Substrate Dynamics of the Epithelial-to-Mesenchymal
747 Transition.,” *Nano Lett.*, vol. 17, no. 5, pp. 3320–3326, May 2017, doi:
748 10.1021/acs.nanolett.7b01558.

749 [60] A. Li *et al.*, “S100A6 promotes the proliferation and migration of cervical cancer cells via
750 the PI3K/Akt signaling pathway.,” *Oncol. Lett.*, vol. 15, no. 4, pp. 5685–5693, Apr. 2018,
751 doi: 10.3892/ol.2018.8018.

752 [61] A. Li *et al.*, “S100A6 promotes cell proliferation in human nasopharyngeal carcinoma via
753 the p38/MAPK signaling pathway.,” *Mol. Carcinog.*, vol. 56, no. 3, pp. 972–984, Mar.
754 2017, doi: 10.1002/mc.22563.

755 [62] P. Li, X. Lv, Z. Zhang, and S. Xie, “S100A6/miR193a regulates the proliferation, invasion,
756 migration and angiogenesis of lung cancer cells through the P53 acetylation.,” *Am. J.*
757 *Transl. Res.*, vol. 11, no. 8, pp. 4634–4649, 2019.

758 [63] B. Haldar *et al.*, “S100A6 is a positive regulator of PPP5C-FKBP51-dependent regulation
759 of endothelial calcium signaling.,” *FASEB J. Off. Publ. Fed. Am. Soc. Exp. Biol.*, vol. 34,
760 no. 2, pp. 3179–3196, Feb. 2020, doi: 10.1096/fj.201901777R.

761 [64] S. Calabretta *et al.*, “Modulation of PKM alternative splicing by PTBP1 promotes
762 gemcitabine resistance in pancreatic cancer cells.,” *Oncogene*, vol. 35, no. 16, pp.
763 2031–2039, Apr. 2016, doi: 10.1038/onc.2015.270.

764 [65] N. Lu, S. Carracedo, J. Ranta, R. Heuchel, R. Soininen, and D. Gullberg, “The human α11
765 integrin promoter drives fibroblast-restricted expression in vivo and is regulated by
766 TGF-β1 in a Smad- and Sp1-dependent manner,” *Matrix Biol.*, vol. 29, no. 3, pp. 166–
767 176, Apr. 2010, doi: 10.1016/j.matbio.2009.11.003.

768 [66] F. Cheng *et al.*, “Vimentin coordinates fibroblast proliferation and keratinocyte
769 differentiation in wound healing via TGF-β-Slug signaling,” *Proc. Natl. Acad. Sci. U. S. A.*,
770 vol. 113, no. 30, pp. E4320–E4327, Jul. 2016, doi: 10.1073/pnas.1519197113.

771 [67] S. J. Serrano-Gomez, M. Maziveyi, and S. K. Alahari, “Regulation of epithelial-
772 mesenchymal transition through epigenetic and post-translational modifications,” *Mol.*
773 *Cancer*, vol. 15, p. 18, Feb. 2016, doi: 10.1186/s12943-016-0502-x.

774 [68] W. Jiao, K. Miyazaki, and Y. Kitajima, “Inverse correlation between E-cadherin and Snail
775 expression in hepatocellular carcinoma cell lines in vitro and in vivo,” *Br. J. Cancer*, vol.

776 86, no. 1, pp. 98–101, 2002, doi: 10.1038/sj.bjc.6600017.

777 [69] I. Poser, D. Domínguez, A. G. de Herreros, A. Varnai, R. Buettner, and A. K. Bosserhoff,
778 "Loss of E-cadherin Expression in Melanoma Cells Involves Up-regulation of the
779 Transcriptional Repressor Snail*," *J. Biol. Chem.*, vol. 276, no. 27, pp. 24661–24666,
780 2001, doi: https://doi.org/10.1074/jbc.M011224200.

781 [70] L. Hao, J. R. Ha, P. Kuzel, E. Garcia, and S. Persad, "Cadherin switch from E- to N-
782 cadherin in melanoma progression is regulated by the PI3K/PTEN pathway through
783 Twist and Snail," *Br. J. Dermatol.*, vol. 166, no. 6, pp. 1184–1197, Jun. 2012, doi:
784 https://doi.org/10.1111/j.1365-2133.2012.10824.x.

785 [71] K. Gravdal, O. J. Halvorsen, S. A. Haukaas, and L. A. Akslen, "A Switch from E-Cadherin
786 to N-Cadherin Expression Indicates Epithelial to Mesenchymal Transition and Is of
787 Strong and Independent Importance for the Progress of Prostate Cancer," *Clin. Cancer*
788 *Res.*, vol. 13, no. 23, pp. 7003 LP – 7011, Dec. 2007, doi: 10.1158/1078-0432.CCR-07-
789 1263.

790 [72] K. Araki *et al.*, "E/N-cadherin switch mediates cancer progression via TGF-β-induced
791 epithelial-to-mesenchymal transition in extrahepatic cholangiocarcinoma," *Br. J.*
792 *Cancer*, vol. 105, no. 12, pp. 1885–1893, 2011, doi: 10.1038/bjc.2011.452.

793 [73] A. B. Roberts *et al.*, "Smad3 is key to TGF-β-mediated epithelial-to-mesenchymal
794 transition, fibrosis, tumor suppression and metastasis," *Cytokine Growth Factor Rev.*,
795 vol. 17, no. 1–2, pp. 19–27, 2006, doi: 10.1016/j.cytogfr.2005.09.008.

796 Supplementary Material and Methods:

797 CRISPR plasmids construction:

798 Single guides RNAs (sgRNAs) for BJ-5ta model were designing using benchling to generate a
799 deletion of 113pb in the exon 3 of *ALMS1* (ENSG00000116127). The 2 sgRNA (5'-
800 CCTAGTCTGGGATGTATCCA – 3' and 5'- GAACAGAAGAGATCTCTGTT – 3') result from benchling
801 were cloned into the plasmid lentiCRISPR v2 [1] following a modified protocol from that
802 described by Shalem et al [2]. LentiCRISPR v2 was a gift from Feng Zhang (Addgene plasmid
803 #52961). Initially, 12.5µL (5µg) of LentiCRISPR V2 were digested with 3µL Esp3I (BsmBI), 3µL
804 FastAP and 6µL 10X FastDigest Buffer from Thermo Fisher. Final volume was set at 60µL. Plasmid
805 digestion was checked by migration in an agarose gel at 1%.

806 sgRNAs were phosphorylated and annealed with its correspondent oligo mixing as follow: 1µL
807 sgRNA (100µM), 1µL of its complement oligo, 2µL of 5X T4 Buffer (Canvax, Cordoba, Spain), 0.5
808 T4 PNK (NEB, Ipswich, EE.UU) and 5.5 µL distilled H_20 (H_2Od). Mix reaction was incubated at 37ºC
809 for 30min and 95ºC for 5min. The samples were then left to stand at room temperature for 2
810 hours and diluted at 1:50, 1:100 and 1:200 ratios.

811 The unpurified digested plasmid was ligated with the diluted sgRNAs as follows: 0.5µL digested
812 LentiCRISPR v2, 2µL diluted sgRNA, 1µL T4 DNA Ligase (Canvax, Cordoba, Spain), 4.5µL H_2Od.
813 The mix was incubated at 37ºC by 30min.

814 Finally, Stable Competent E.coli (NEB, Ipswich, EE.UU) were transformed by thermal shock
815 according to the manufactured protocol and incubated at 30ºC overnight. After that, construct
816 validation was carried out using forward primer for U6 promotor (5'- GACTATCATATGCTTACCGT
817 -3') and reverse sgRNA.

818 Plasmids Transfection and Lentivirus production:

819 293T were seeded in a concentration of $3x10^5$ into a 6-well plate and incubated overnight. Then,
820 293T cells were co-transfected with each CRISPR construct and the plasmids psPAX2 and pCMV-
821 VSV-G [3] using lipofectamine 3000 (Thermo Fisher, Waltham, EE. UU). pCMV-VSV-G was a gift
822 from Bob Weinberg (Addgene plasmid #8454) and psPAX2 was a gift from Didier Trono (Addgene
823 plasmid #12260)

824 Initially, 7.5µL of lipofectamine 3000 were diluted in 125µL of Opti-MEM medium (Thermo
825 Fisher, Waltham, EE. UU) by duplicate. Then a total amount of 5µg of ADN (1.6µL for each
826 plasmid) were diluted at 250µL Opti-MEM. After that, diluted DNA and diluted lipofectamine
827 were mixed in a 1:1 ratio, centrifugated at 1200rpm and incubated for 20min at room
828 temperature. Finally, the 250µL of mix were applied to the wells containing the cells.

829 The cells were incubated with the mixture for 24 hours. Then, the mixture was removed and the
830 cell was cultured for a further 72 hours for lentivirus production.

831 Lentiviral transduction:

832 After 72 hours of culturing 293T cells transfected for lentivirus production, the culture medium
833 was collected in 15 mL tubes and filtered through a 45µm filter (Sartorious,). In addition, a
834 solution of complete DMEM medium without P/S with polybrene was prepared at a dilution of
835 1:1000 (8µg/ml).

836 Then, 300µL lentiviral preparation were mixed with 200µL complete DMEM médium with
837 polybrene for each well. An additional 1 ml of DMEM with polybrene was added and the plates
838 were centrifuged at 800g for 30 minutes. This step was repeated one more time. After the
839 second centrifugation the mix with lentivirus was added again and the plates were incubated
840 for 24 hours. Finally, mix was removed and cells were allowed to settle for 48 hours in DMEM
841 médium. They were then selected with puromycin (1ng/mL) for 5 days.

842 Edition validation:

843 After puromycin selection, clonal isolation and expansion we checked the lack of *ALMS1* gene
844 by qPCR in StepOnePlus (Thermo Fisher, Waltham, EE. UU). Finally, we found that these cells
845 had the expected exon 3 deletion by PCR with resolution of samples on a 2% agarose gel and
846 followed by sanger sequencing.

847

Supplementary figures:

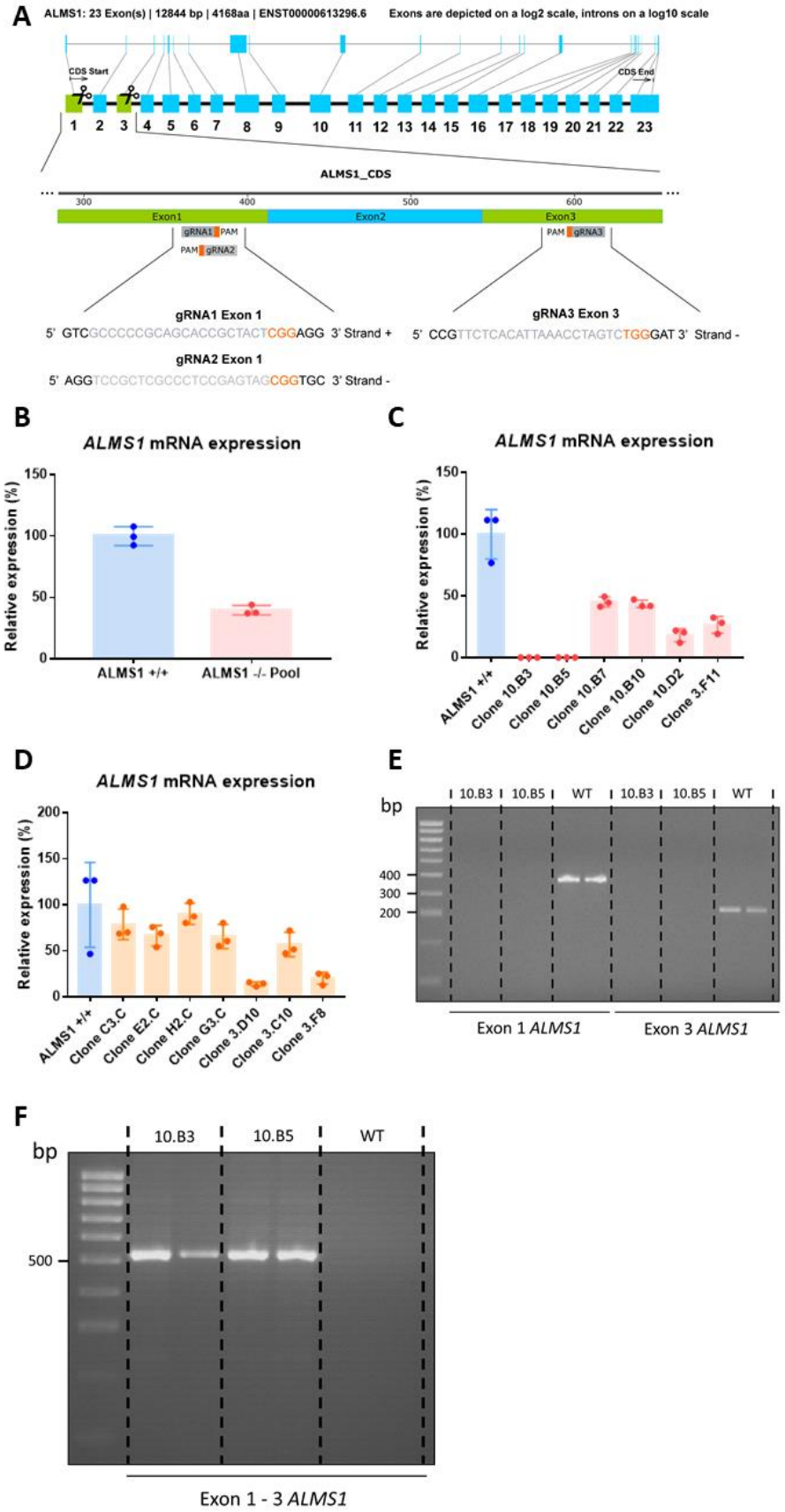

850 **Supplementary Figure S1.** Characterisation of *ALMS1* -/- cell line HeLa. **(A)** Design of the model.
851 **(B)** Relative gene expression of *ALMS1 +/+* and polyclonal cell line for *ALMS1 -/-* genotype. **(C)**
852 Relative gene expression of ALMS1 +/+ and a first batch of clones for *ALMS1 -/-* genotype. **(D)**
853 Relative gene expression of ALMS1 +/+ and second batch of clones for ALMS1 -/- genotype. **(E)**
854 Strategy for amplification of exons 1 and 3 from genomic DNA in two clones of the *ALMS1* -/-
855 (KO) line and the *ALMS1* +/+ control (WT). **(F)** Amplification strategy of the resulting sequence
856 between exon 1 and 3 after removal of the sequencing between the 2 outermost gRNAs.

857

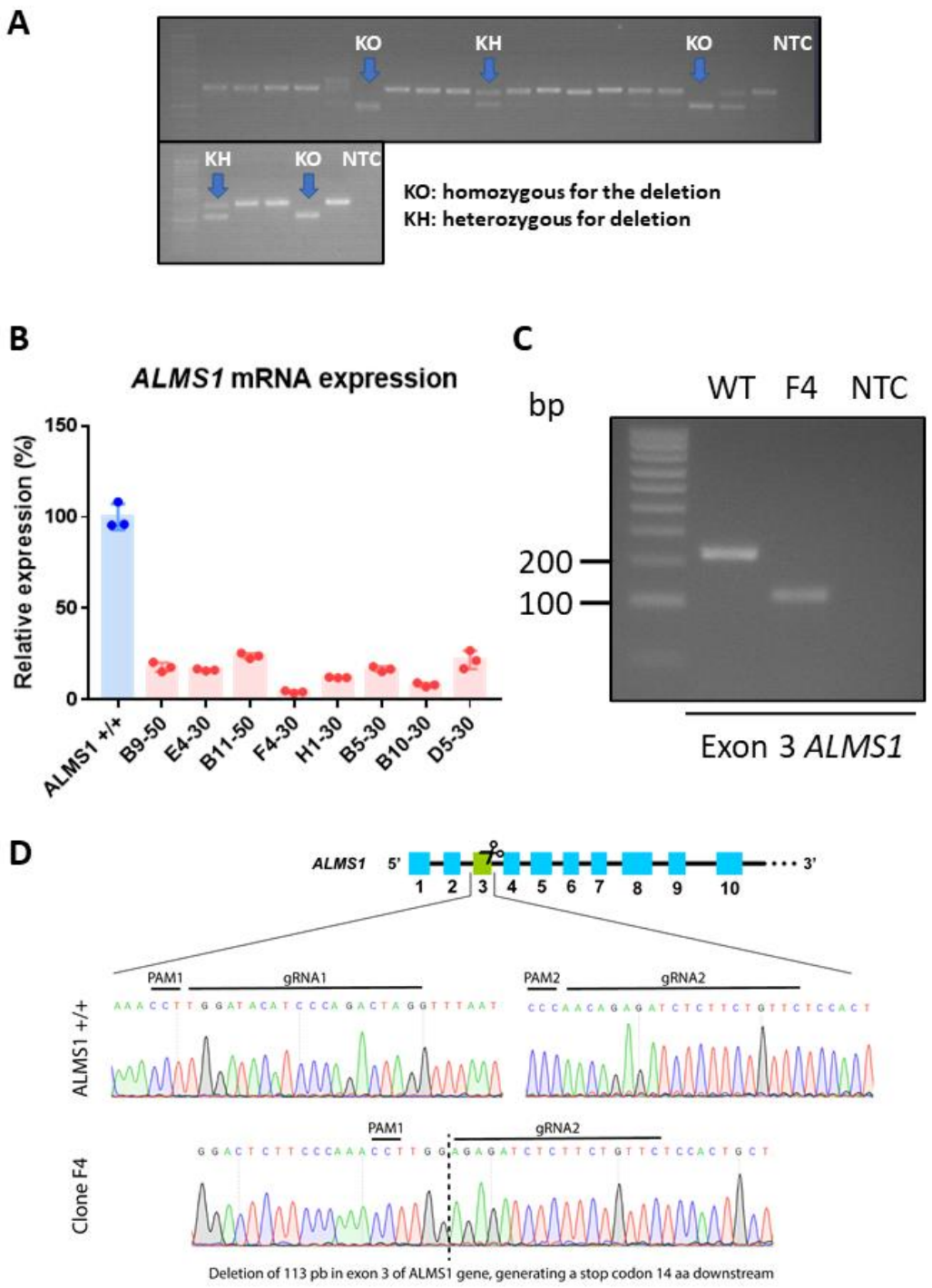

858

859 **Supplementary Figure S2.** Genetic characterisation of *ALMS1* -/- cell line BJ-5ta. **(A)** Clone
860 screening. **(B)** Relative gene expression of ALMS1 +/+ and a batch of clones for ALMS1 -/-
861 genotype. **(C)** Agarose gel (2%) showing the exon 3 amplicon of the control line (ALMS1 +/+) and
862 the F4 clone (ALMS1 -/-) which showed the lowest gene expression. **(D)** Characterisation of the
863 F4 clone mutation by sanger sequencing.

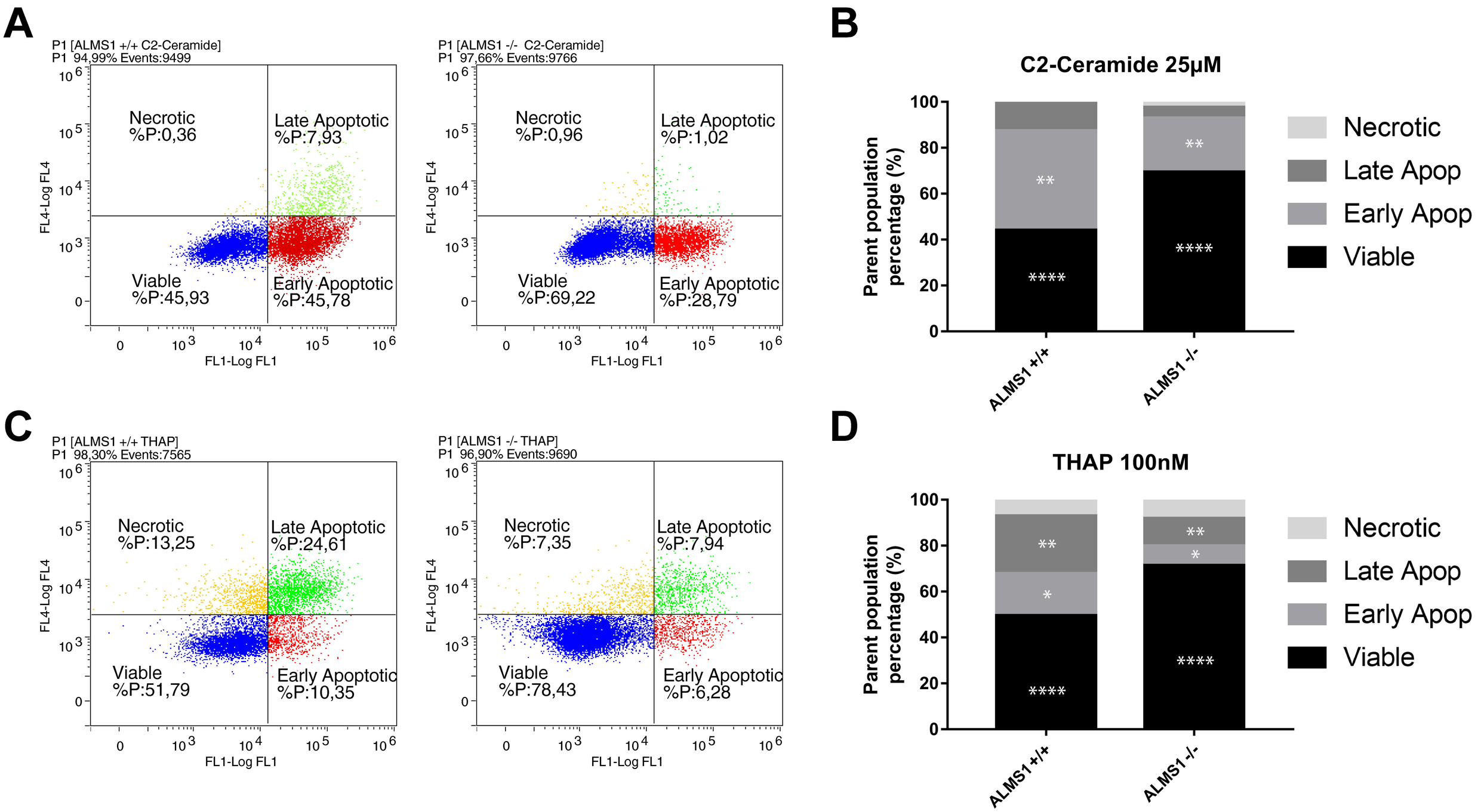
A
P1 [ALMS1 +/+ C2-Ceramide]
P1 94,99% Events:9499
Necrotic
%P:0,36
Late Apoptotic
%P:7,93
Viable
%P:45,93
Early Apoptotic
%P:45,78
P1 [ALMS1 -/- C2-Ceramide]
P1 97,66% Events:9766
Necrotic
%P:0,96
Late Apoptotic
%P:1,02
Viable
%P:69,22
Early Apoptotic
%P:28,79
FL4-Log FL4
FL1-Log FL1
B
C2-Ceramide 25µM
Parent population percentage (%)
ALMS1 +/+
ALMS1 -/-
Necrotic
Late Apop
Early Apop
Viable
C
P1 [ALMS1 +/+ THAP]
P1 98,30% Events:7565
Necrotic
%P:13,25
Late Apoptotic
%P:24,61
Viable
%P:51,79
Early Apoptotic
%P:10,35
P1 [ALMS1 -/- THAP]
P1 96,90% Events:9690
Necrotic
%P:7,35
Late Apoptotic
%P:7,94
Viable
%P:78,43
Early Apoptotic
%P:6,28
D
THAP 100nM

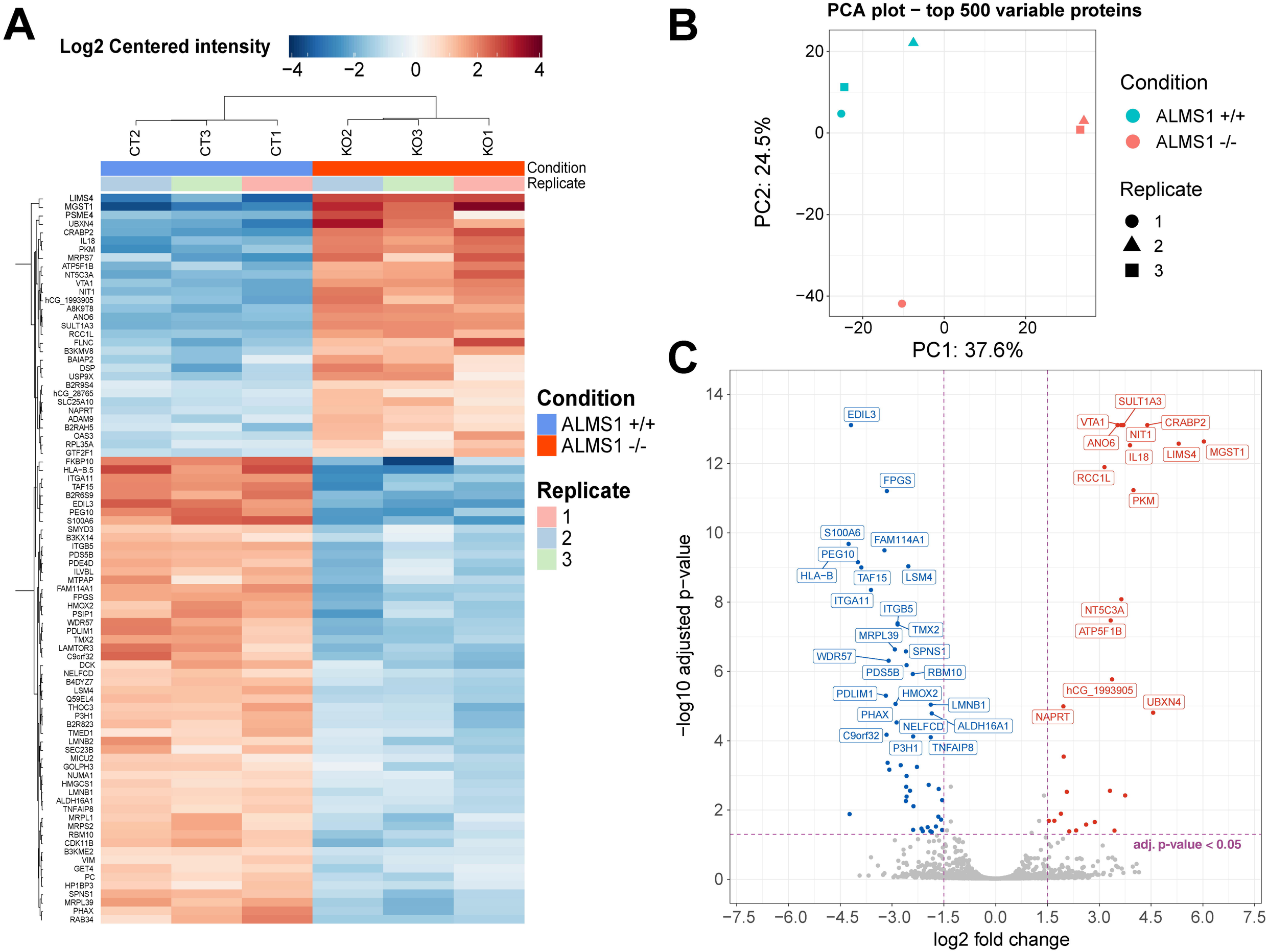
A
Log2 Centered intensity
−4
−2
0
2
4
CT2
CT3
CT1
KO2
KO3
KO1
Condition
Replicate
Condition
ALMS1 +/+
ALMS1 -/-
Replicate
1
2
3
B
PCA plot − top 500 variable proteins
PC2: 24.5%
PC1: 37.6%
Condition
ALMS1 +/+
ALMS1 -/-
Replicate
1
2
3
C
−log10 adjusted p−value
log2 fold change
adj. p-value < 0.05
EDIL3
FPGS
S100A6
FAM114A1
PEG10
HLA−B
TAF15
LSM4
ITGA11
ITGB5
TMX2
MRPL39
SPNS1
WDR57
PDS5B
RBM10
PDLIM1
HMOX2
LMNB1
PHAX
NELFCD
ALDH16A1
C9orf32
P3H1
TNFAIP8
SULT1A3
VTA1
CRABP2
NIT1
ANO6
IL18
LIMS4
MGST1
RCC1L
PKM
NT5C3A
ATP5F1B
hCG_1993905
UBXN4
NAPRT

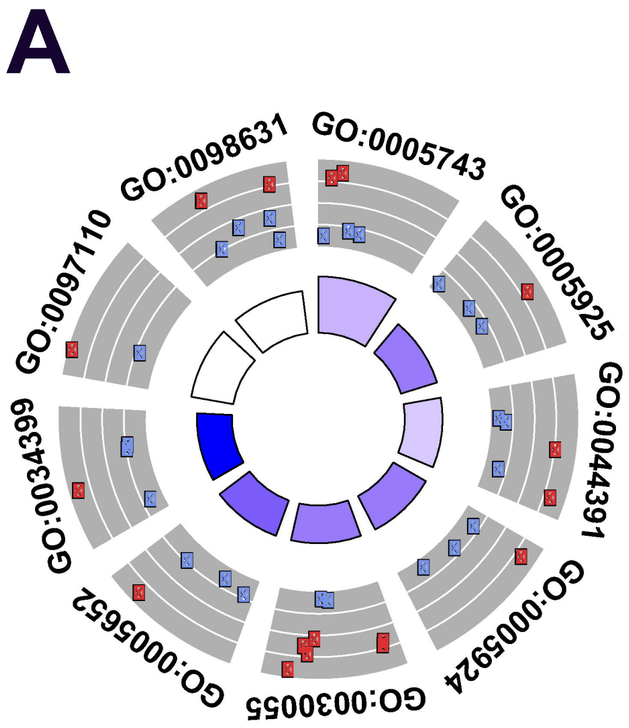

ID	Description
GO:0005743	Mitochondrial inner membrane
GO:0005925	Focal adhesion
GO:0044391	Ribosomal subunit
GO:0005924	Cell−substrate adherens junction
GO:0030055	Cell−substrate junction
GO:0005652	Nuclear lamina
GO:0034399	Nuclear periphery
GO:0097110	Scaffold protein binding
GO:0098631	Cell adhesion mediator activity

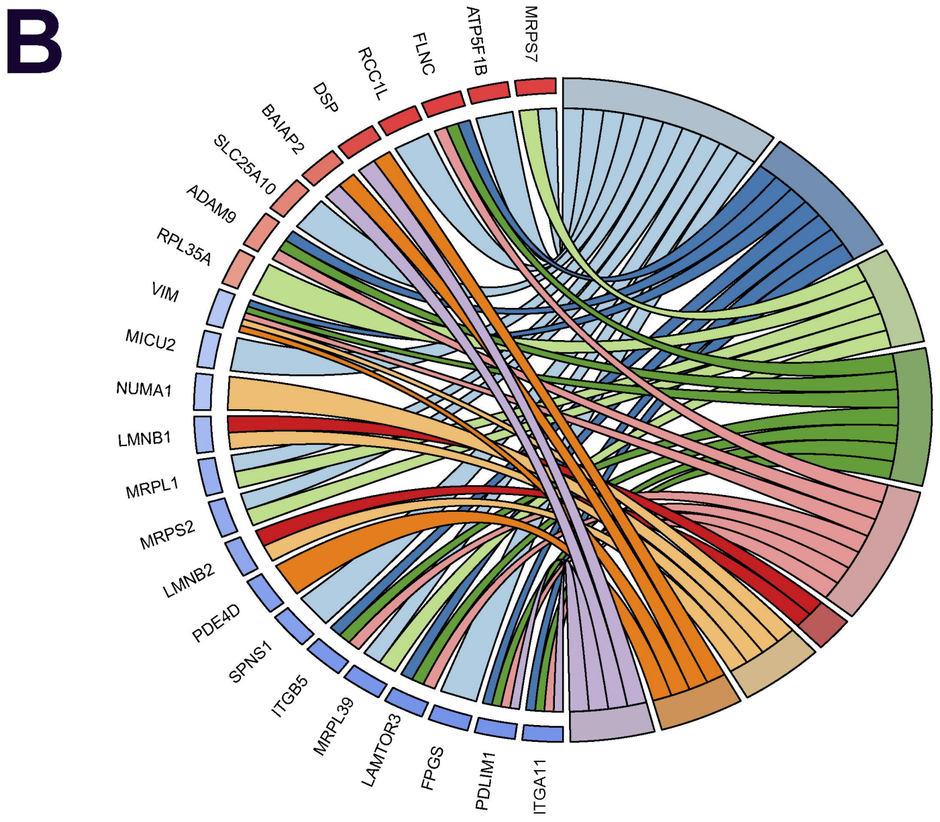

Z−score

Decreasing — Increasing

Log2FC

Downregulated

Upregulated

Log2FC

3

−3

GO Terms

- Mitochondrial inner membrane
- Focal adhesion
- Ribosomal subunit
- Cell−substrate adherens junction
- Cell−substrate junction
- Nuclear lamina
- Nuclear periphery
- Scaffold protein binding
- Cell adhesion mediator activity

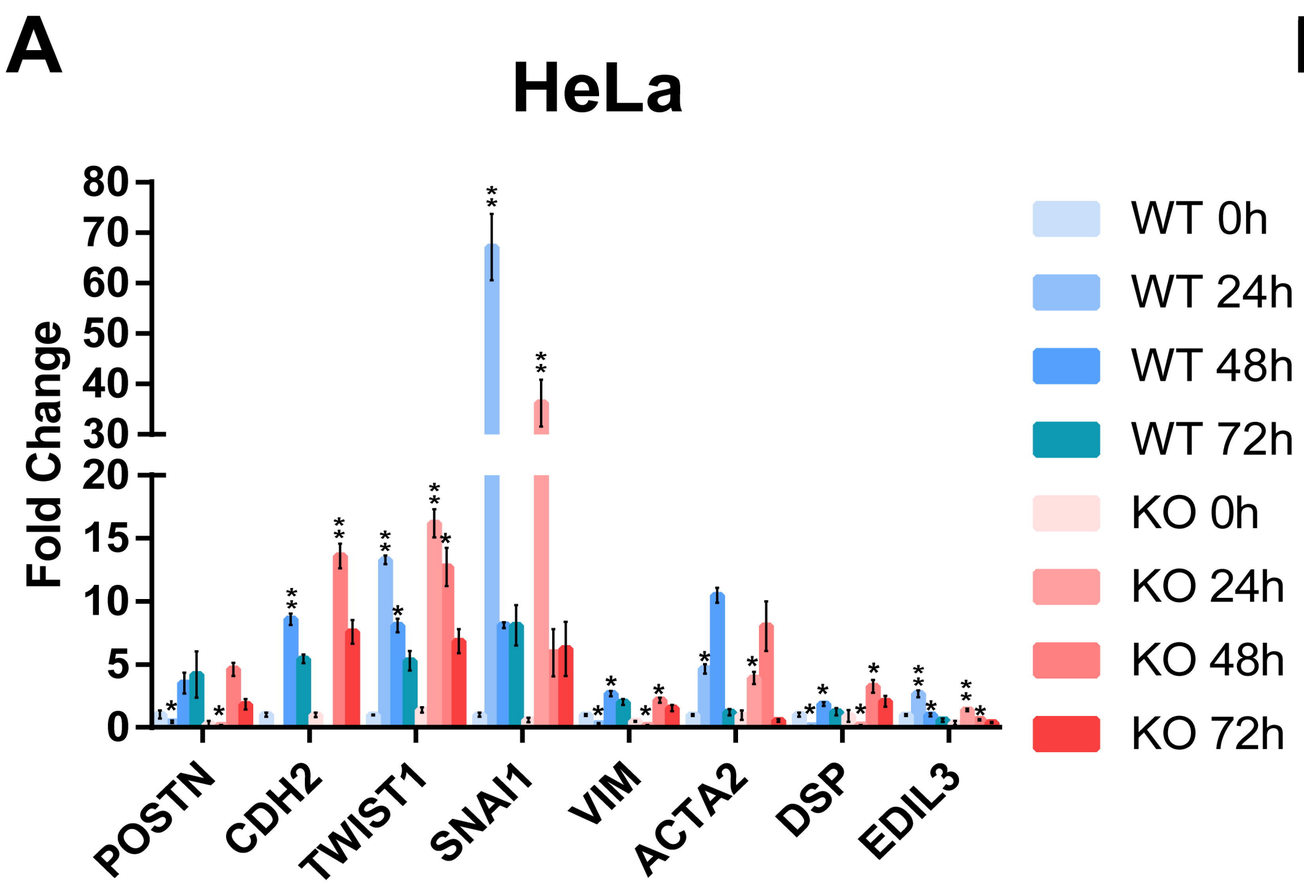
A
HeLa
Fold Change
80
70
60
50
40
30
20
15
10
5
0
POSTN
CDH2
TWIST1
SNAI1
VIM
ACTA2
DSP
EDIL3
WT 0h
WT 24h
WT 48h
WT 72h
KO 0h
KO 24h
KO 48h
KO 72h

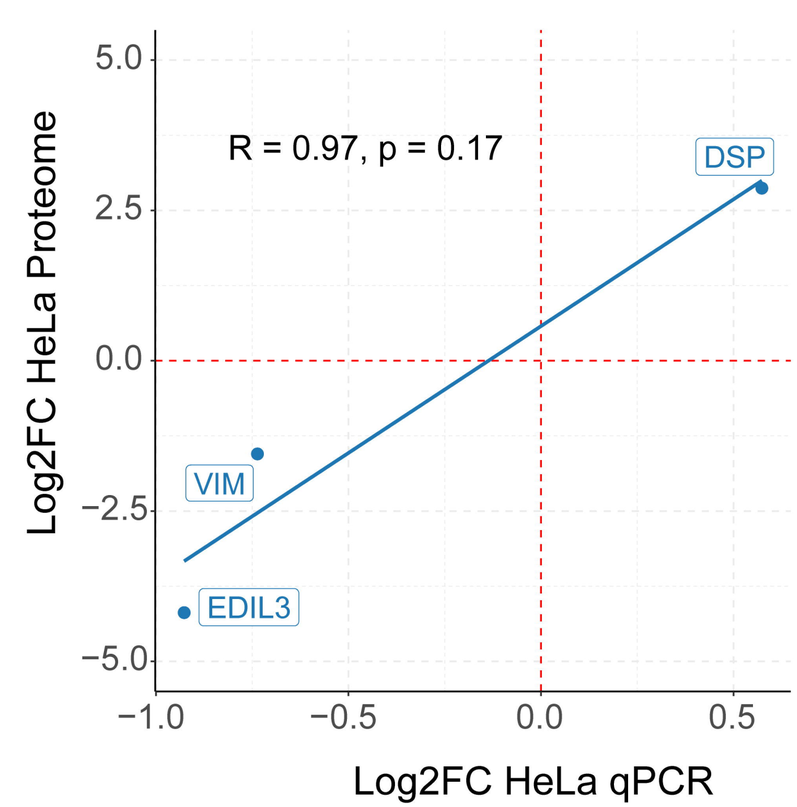
B
R = 0.97, p = 0.17
DSP
VIM
EDIL3
Log2FC HeLa Proteome
5.0
2.5
0.0
−2.5
−5.0
−1.0
−0.5
0.0
0.5
Log2FC HeLa qPCR

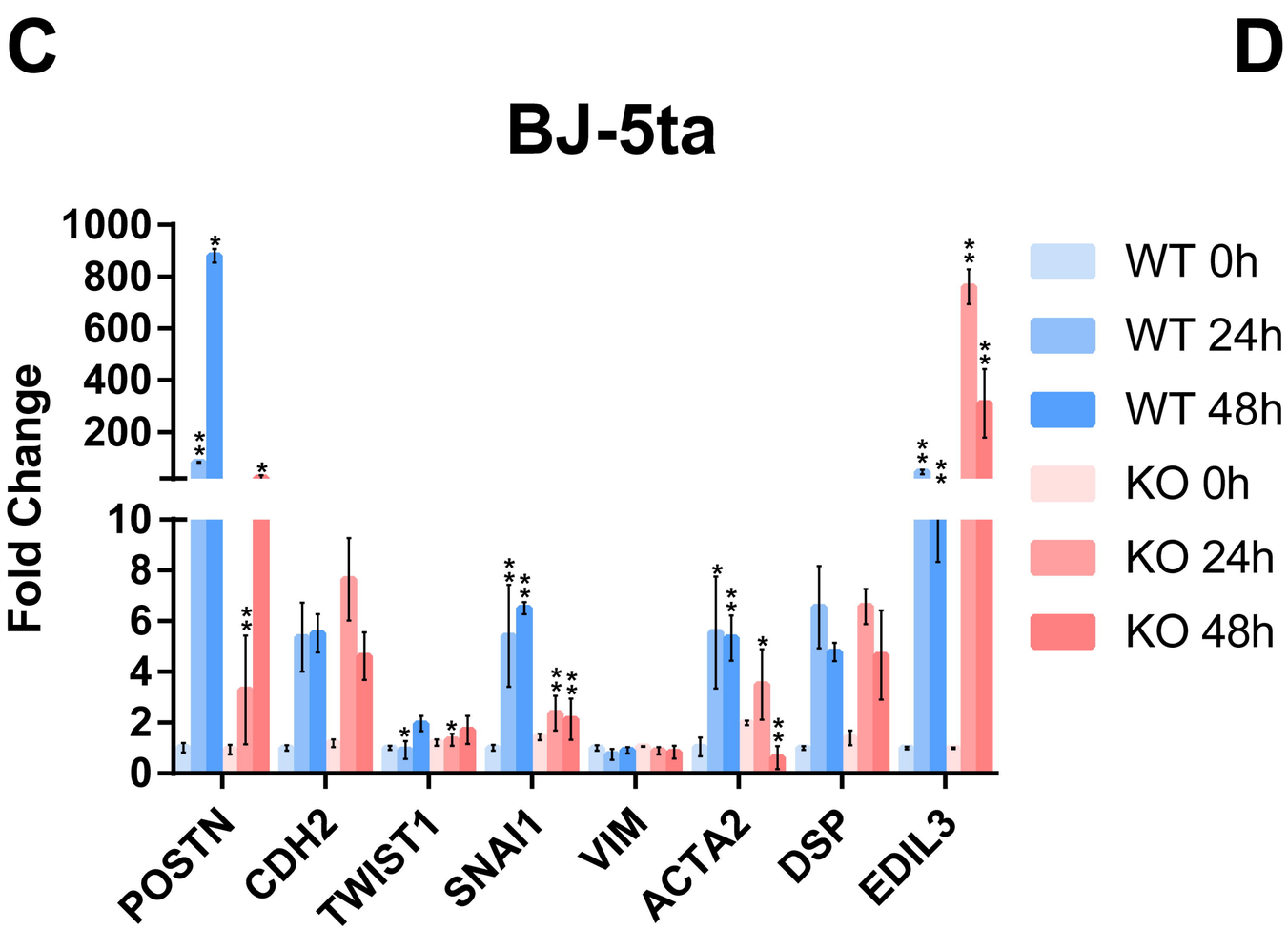
C
BJ-5ta
Fold Change
1000
800
600
400
200
10
8
6
4
2
0
POSTN
CDH2
TWIST1
SNAI1
VIM
ACTA2
DSP
EDIL3
WT 0h
WT 24h
WT 48h
KO 0h
KO 24h
KO 48h

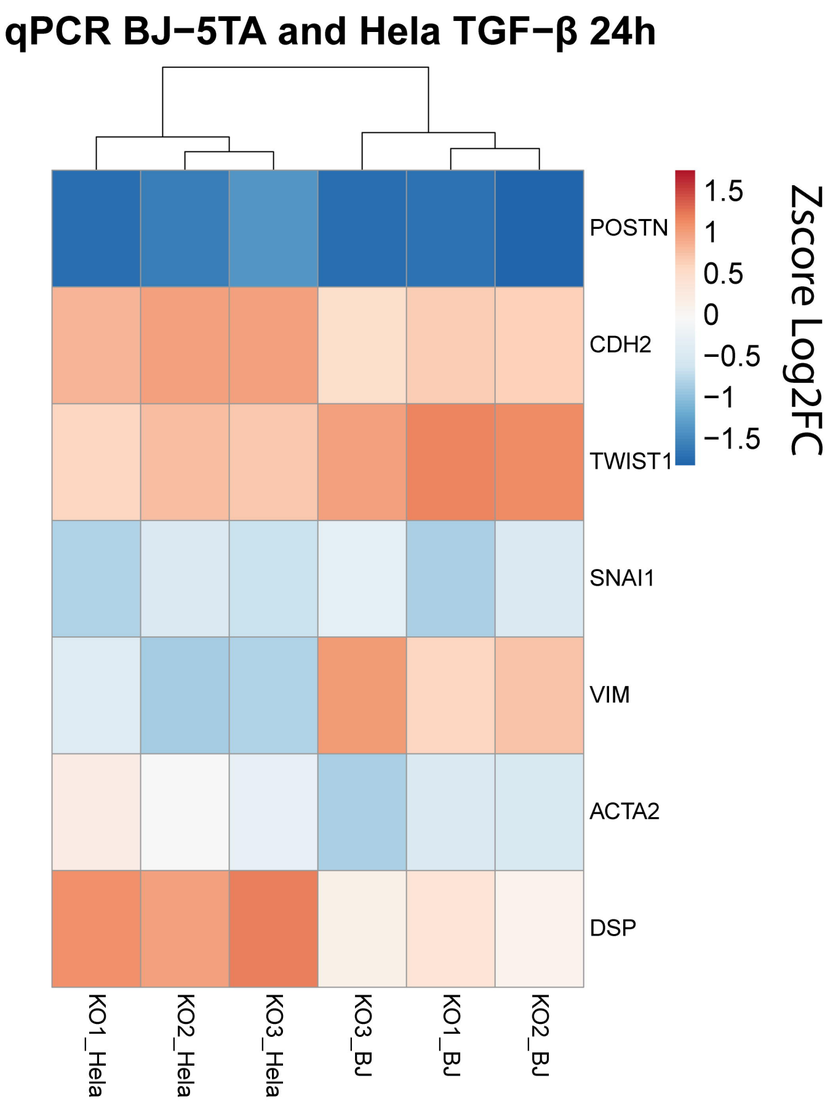
D
qPCR BJ−5TA and Hela TGF−β 24h
POSTN
CDH2
TWIST1
SNAI1
VIM
ACTA2
DSP
KO1_Hela
KO2_Hela
KO3_Hela
KO3_BJ
KO1_BJ
KO2_BJ
Zscore Log2FC
1.5
1
0.5
0
−0.5
−1
−1.5

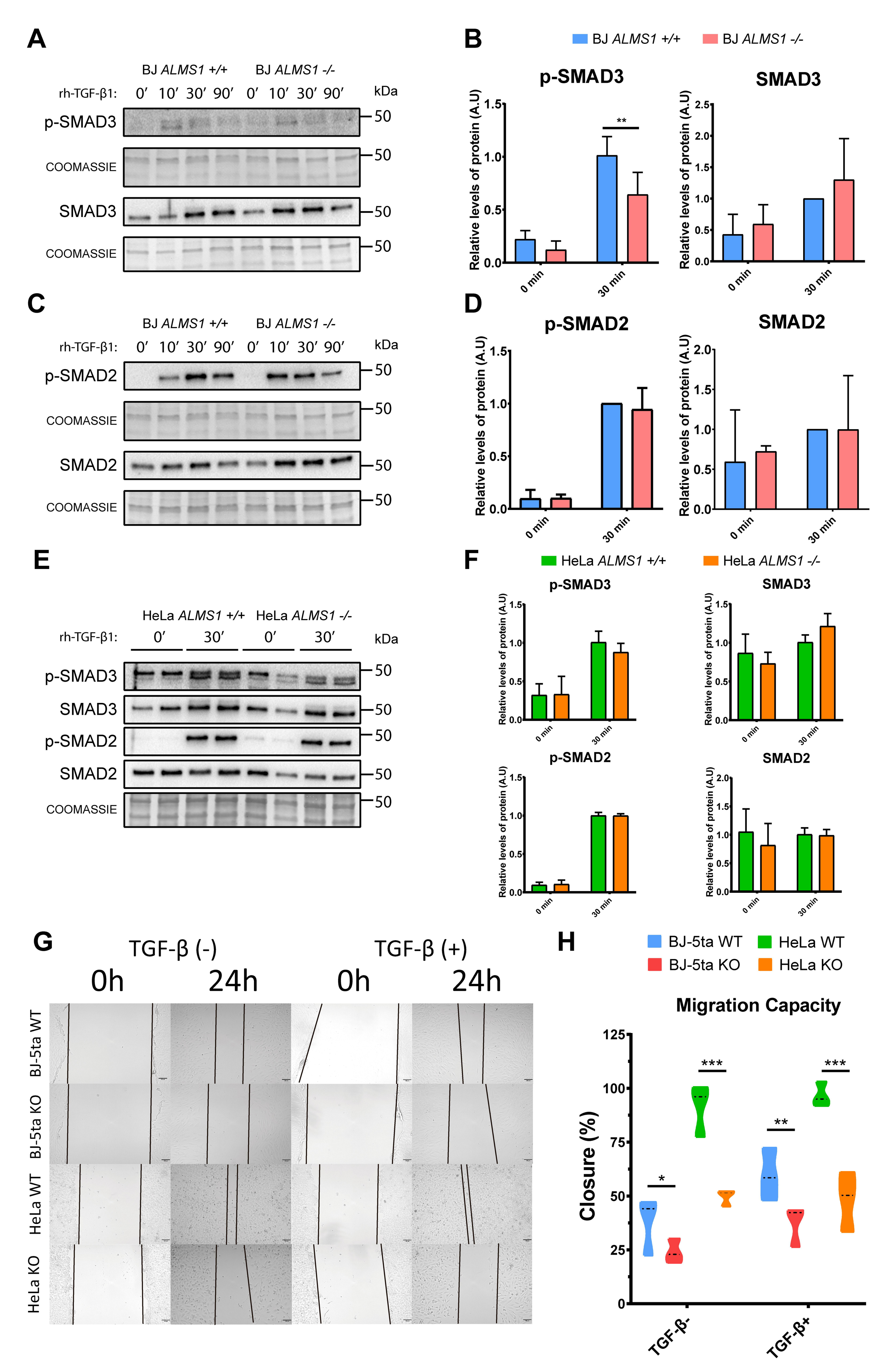
A
BJ ALMS1 +/+
BJ ALMS1 -/-
rh-TGF-β1: 0′ 10′ 30′ 90′ 0′ 10′ 30′ 90′
kDa
p-SMAD3
COOMASSIE
SMAD3
COOMASSIE
50
B
BJ ALMS1 +/+
BJ ALMS1 -/-
p-SMAD3
SMAD3
Relative levels of protein (A.U)
0 min
30 min
**
C
BJ ALMS1 +/+
BJ ALMS1 -/-
rh-TGF-β1: 0′ 10′ 30′ 90′ 0′ 10′ 30′ 90′
kDa
p-SMAD2
COOMASSIE
SMAD2
COOMASSIE
D
p-SMAD2
SMAD2
Relative levels of protein (A.U)
0 min
30 min
E
HeLa ALMS1 +/+
HeLa ALMS1 -/-
rh-TGF-β1: 0′ 30′ 0′ 30′
kDa
p-SMAD3
SMAD3
p-SMAD2
SMAD2
COOMASSIE
F
HeLa ALMS1 +/+
HeLa ALMS1 -/-
p-SMAD3
SMAD3
p-SMAD2
SMAD2
Relative levels of protein (A.U)
0 min
30 min
G
TGF-β (-)
TGF-β (+)
0h
24h
0h
24h
BJ-5ta WT
BJ-5ta KO
HeLa WT
HeLa KO
H
BJ-5ta WT
HeLa WT
BJ-5ta KO
HeLa KO
Migration Capacity
Closure (%)
TGF-β-
TGF-β+
*
**
***

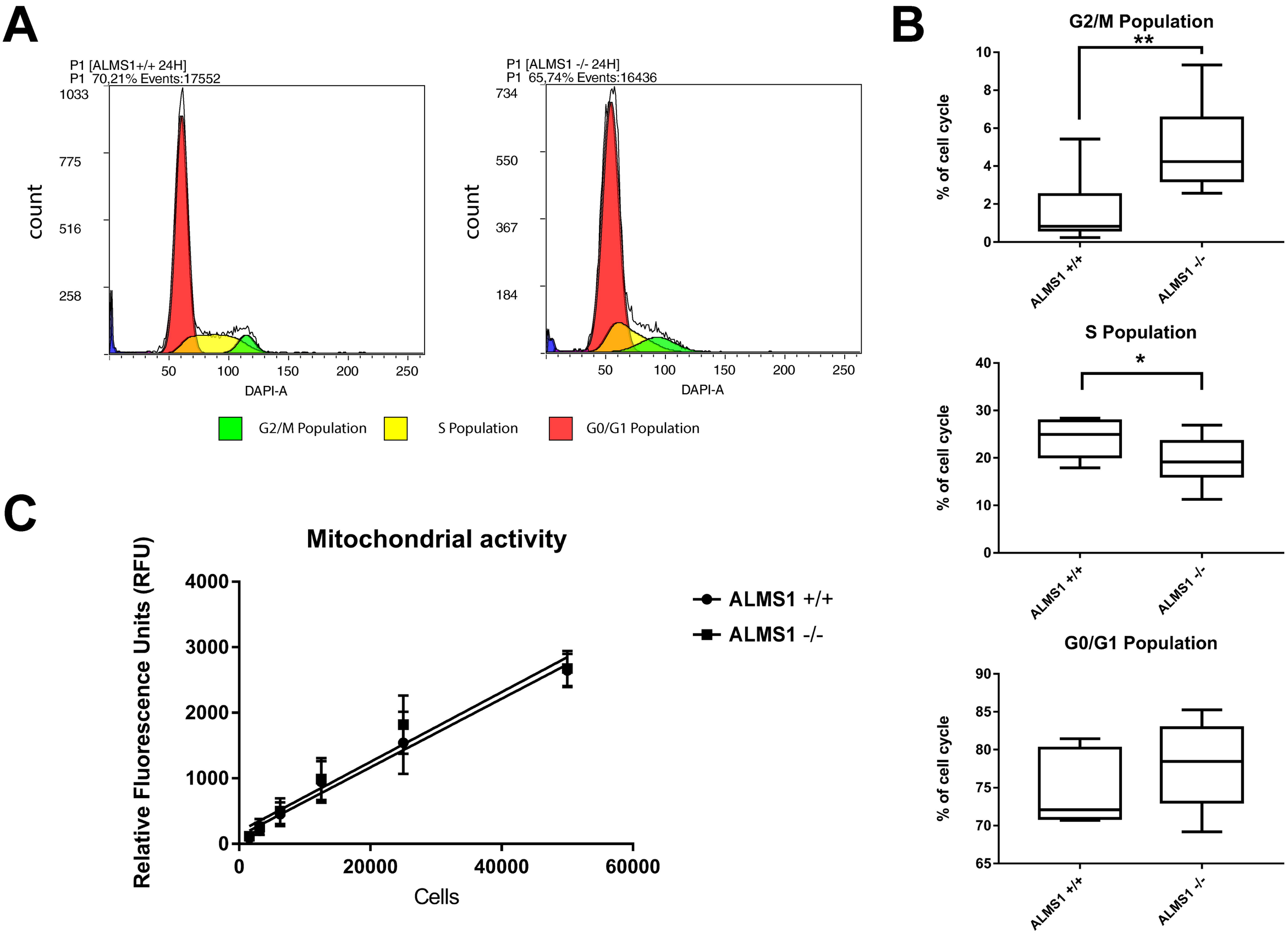
A
P1 [ALMS1+/+ 24H]
P1 70,21% Events:17552
count
1033
775
516
258
50
100
150
200
250
DAPI-A
P1 [ALMS1 -/- 24H]
P1 65,74% Events:16436
count
734
550
367
184
50
100
150
200
250
DAPI-A
G2/M Population
S Population
G0/G1 Population
B
G2/M Population
**
% of cell cycle
10
8
6
4
2
0
ALMS1 +/+
ALMS1 -/-
S Population
*
% of cell cycle
40
30
20
10
0
ALMS1 +/+
ALMS1 -/-
G0/G1 Population
% of cell cycle
90
85
80
75
70
65
ALMS1 +/+
ALMS1 -/-
C
Mitochondrial activity
Relative Fluorescence Units (RFU)
4000
3000
2000
1000
0
0
20000
40000
60000
Cells
ALMS1 +/+
ALMS1 -/-

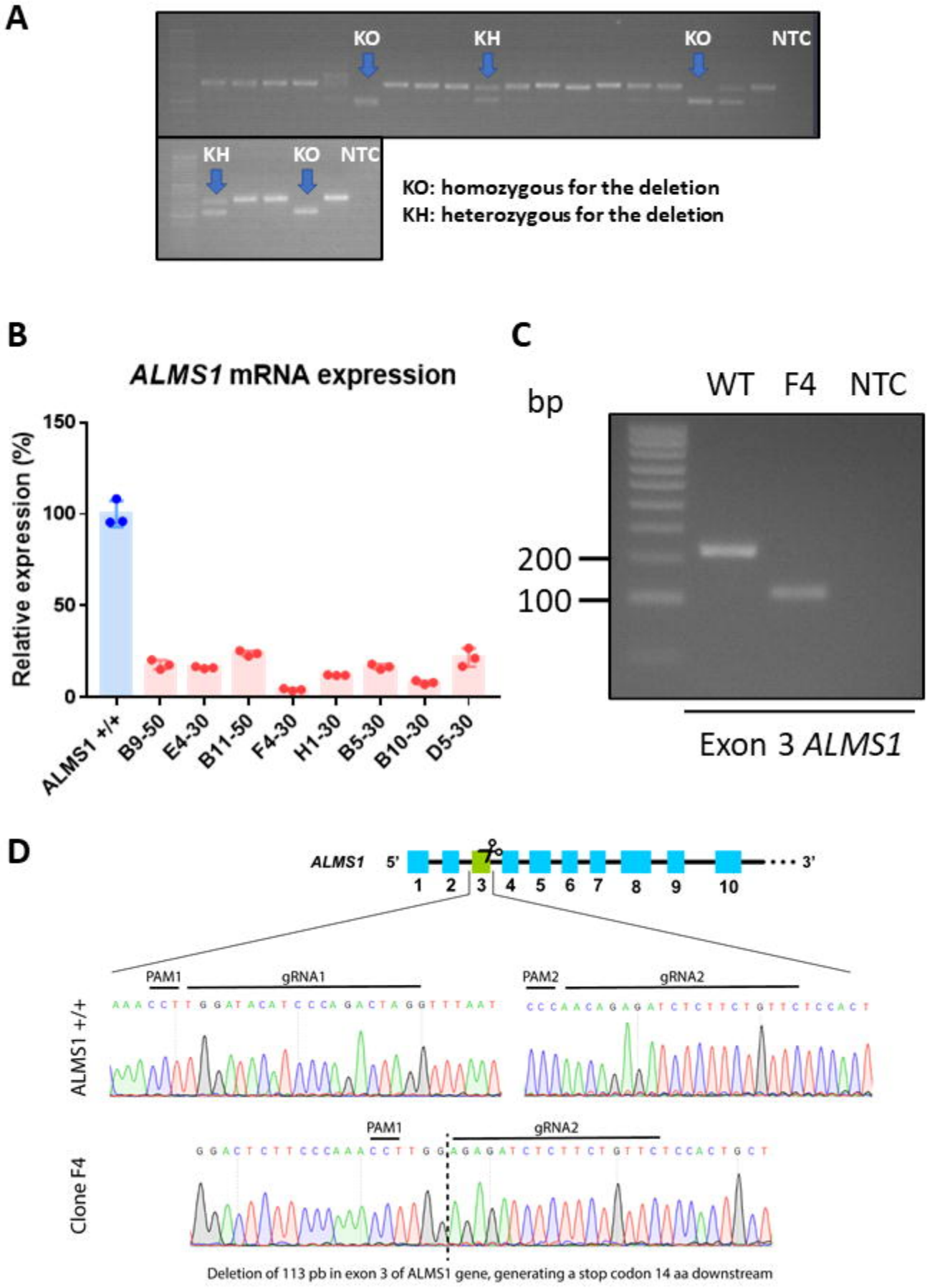
A
KO
KH
KO
NTC
KH
KO
NTC
KO: homozygous for the deletion
KH: heterozygous for the deletion
B
ALMS1 mRNA expression
Relative expression (%)
150
100
50
0
ALMS1 +/+
B9-50
E4-30
B11-50
F4-30
H1-30
B5-30
B10-30
D5-30
C
bp
WT
F4
NTC
200
100
Exon 3 ALMS1
D
ALMS1
5'
3'
1
2
3
4
5
6
7
8
9
10
PAM1
gRNA1
PAM2
gRNA2
ALMS1 +/+
PAM1
gRNA2
Clone F4
Deletion of 113 pb in exon 3 of ALMS1 gene, generating a stop codon 14 aa downstream

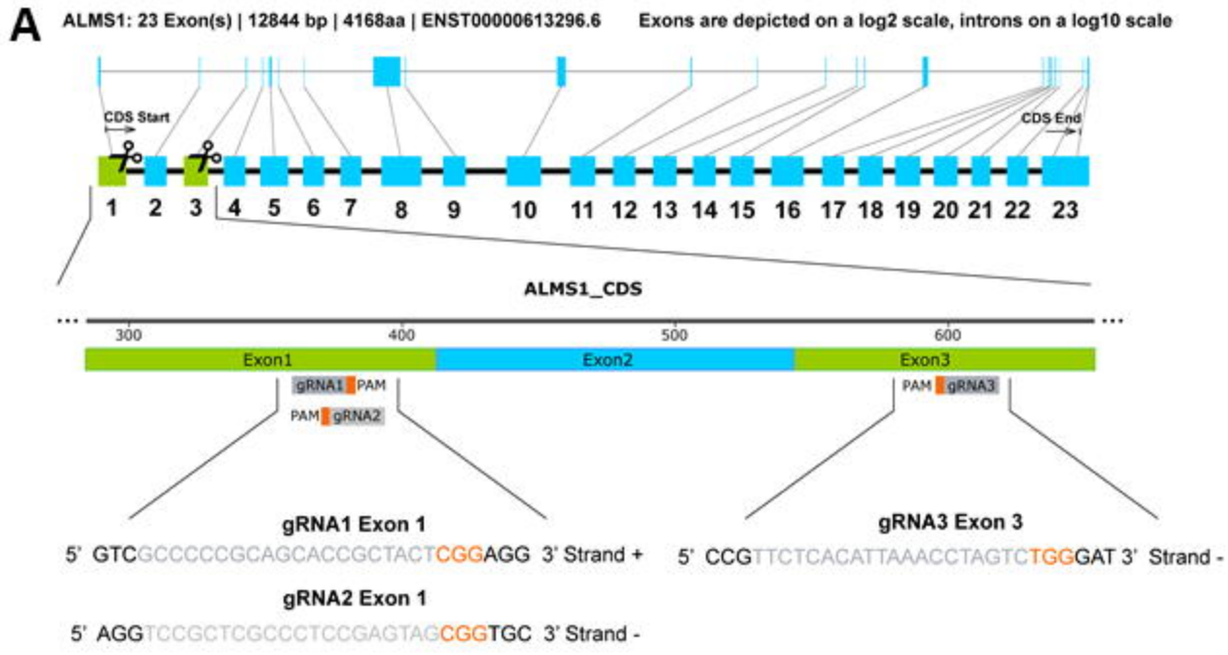
A
ALMS1: 23 Exon(s) | 12844 bp | 4168aa | ENST00000613296.6
Exons are depicted on a log2 scale, introns on a log10 scale
CDS Start
CDS End
1 2 3 4 5 6 7 8 9 10 11 12 13 14 15 16 17 18 19 20 21 22 23
ALMS1_CDS
300 400 500 600
Exon1
Exon2
Exon3
gRNA1 PAM
PAM gRNA2
PAM gRNA3
gRNA1 Exon 1
5' GTCGCCCCCGCAGCACCGCTACTCGGAGG 3' Strand +
gRNA3 Exon 3
5' CCGTTCTCACATTAAACCTAGTCTGGGAT 3' Strand -
gRNA2 Exon 1
5' AGGTCCGCTCGCCCTCCGAGTAGCGGTGC 3' Strand -

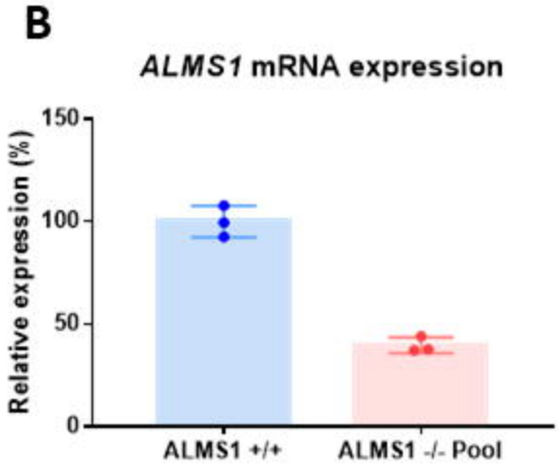
B
ALMS1 mRNA expression
Relative expression (%)
150
100
50
0
ALMS1 +/+
ALMS1 -/- Pool

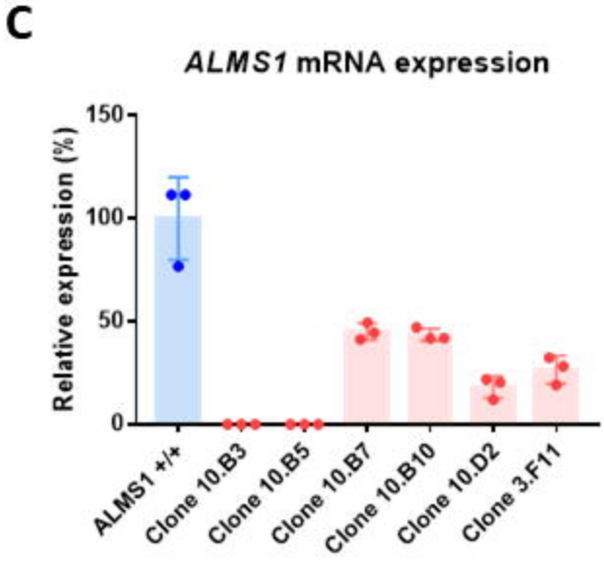
C
ALMS1 mRNA expression
Relative expression (%)
150
100
50
0
ALMS1 +/+
Clone 10.B3
Clone 10.B5
Clone 10.B7
Clone 10.B10
Clone 10.D2
Clone 3.F11

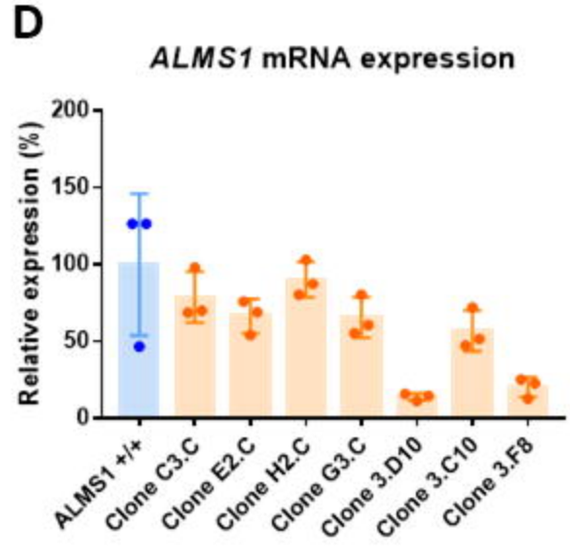
D
ALMS1 mRNA expression
Relative expression (%)
200
150
100
50
0
ALMS1 +/+
Clone C3.C
Clone E2.C
Clone H2.C
Clone G3.C
Clone 3.D10
Clone 3.C10
Clone 3.F8

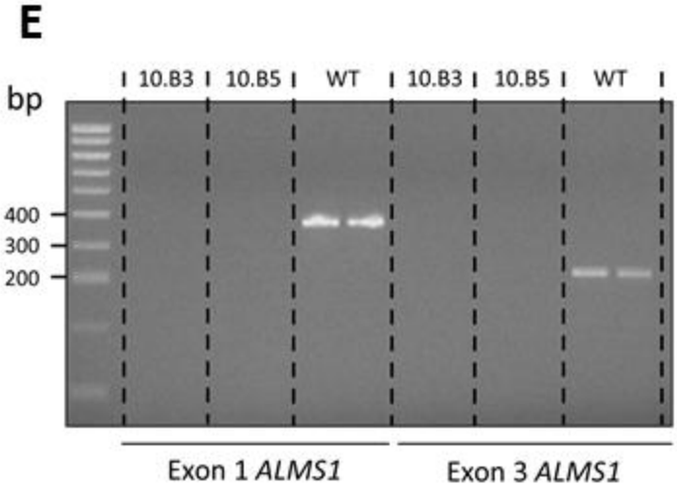
E
bp
10.B3
10.B5
WT
10.B3
10.B5
WT
400
300
200
Exon 1 ALMS1
Exon 3 ALMS1

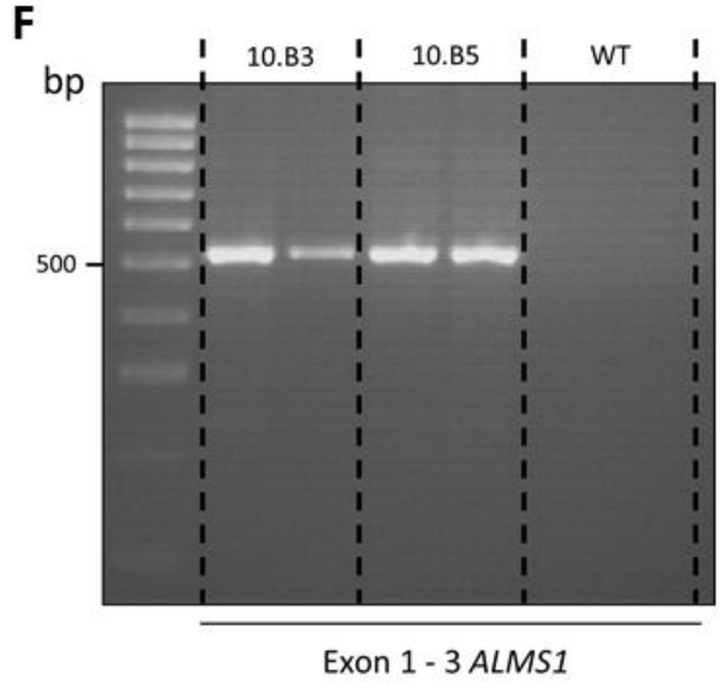
F
bp
10.B3
10.B5
WT
500
Exon 1 - 3 ALMS1